HAL
open science

Chemical weathering and consumption of atmospheric carbon dioxide in the Alpine region

Marco Donnini, Francesco Frondini, Jean-Luc Probst, Anne Probst, Carlo Cardellini, Ivan Marchesini, Fausto Guzzetti

To cite this version:

Marco Donnini, Francesco Frondini, Jean-Luc Probst, Anne Probst, Carlo Cardellini, et al.. Chemical weathering and consumption of atmospheric carbon dioxide in the Alpine region. Global and Planetary Change, 2016, vol. 136, pp. 65-81. 10.1016/j.gloplacha.2015.10.017 . hal-01252822

HAL Id: hal-01252822

https://hal.science/hal-01252822v1

Submitted on 8 Jan 2016

HAL is a multi-disciplinary open access archive for the deposit and dissemination of scientific research documents, whether they are published or not. The documents may come from teaching and research institutions in France or abroad, or from public or private research centers.

L'archive ouverte pluridisciplinaire **HAL**, est destinée au dépôt et à la diffusion de documents scientifiques de niveau recherche, publiés ou non, émanant des établissements d'enseignement et de recherche français ou étrangers, des laboratoires publics ou privés.

Open Archive TOULOUSE Archive Ouverte (OATAO)
OATAO is an open access repository that collects the work of Toulouse researchers and makes it freely available over the web where possible.

This is an author-deposited version published in : http://oatao.univ-toulouse.fr/
Eprints ID : 14623

To link to this article : DOI:10.1016/j.gloplacha.2015.10.017
URL : http://dx.doi.org/10.1016/j.gloplacha.2015.10.017

To cite this version : Donnini, Marco and Frondini, Francesco and Probst, Jean-Luc and Probst, Anne and Cardellini, Carlo and Marchesini, Ivan and Guzzetti, Fausto *Chemical weathering and consumption of atmospheric carbon dioxide in the Alpine region.* (2016) Global and Planetary Change, vol. 136. pp. 65-81. ISSN 09218181

Any correspondance concerning this service should be sent to the repository administrator: staff-oatao@listes-diff.inp-toulouse.fr

Chemical weathering and consumption of atmospheric carbon dioxide in the Alpine region

Marco Donnini [a,d,*], Francesco Frondini [a], Jean-Luc Probst [b,c], Anne Probst [b,c], Carlo Cardellini [a], Ivan Marchesini [d], Fausto Guzzetti [d]

[a] Università degli Studi di Perugia, Dipartimento di Fisica e Geologia, Perugia, Italy
[b] University of Toulouse, INPT, UPS, Laboratorie Ecologie Fonctionnelle et Environment (EcoLab), ENSAT, Castanet Tolosan, France
[c] Centre National de la Recherche Scientifique (CNRS), EcoLab, ENSAT, Castanet Tolosan, France
[d] Consiglio Nazionale delle Ricerche (CNR), Istituto di Ricerca per la Protezione Idrogeologica, Perugia, Italy

ARTICLE INFO

Article history:
Received 25 May 2015
Received in revised form 26 September 2015
Accepted 30 October 2015
Available online 31 October 2015

Keywords:
Chemical weathering
Carbon dioxide
Alps
Rivers
Runoff

ABSTRACT

To determine the CO_2 consumption due to chemical weathering in the Alps, water samples from the 32 main Alpine rivers were collected and analysed in two periods, spring 2011 and winter 2011/2012. Most of the river waters are characterized by a bicarbonate earth-alkaline composition with some samples showing a clear enrichment in sulphates and other samples showing a slight enrichment in alkaline metals. The amount of total dissolved solids (TDS) ranges between 96 and 551 mg/L. Considering the major ion composition and the Sr isotopic composition of water samples, coherently with the geological setting of the study area, three major reservoirs of dissolved load have been recognized: carbonates, evaporites and silicates. Based on a chemical mass balance, the flux of dissolved solids, and the flux of carbon dioxide consumed by chemical weathering have been computed for each basin and for the entire study area. Results show that the flux of dissolved solids, ranges from 8×10^3 to 411×10^3 kg km^{-2} y^{-1}, with an average value of 127×10^3 kg km^{-2} y^{-1}, while the flux of carbon dioxide consumed by chemical weathering in the short-term (<1 Ma) is 5.03×10^5 mol km^{-2} y^{-1} 1 on average. Since part of the CO_2 is returned to the atmosphere through carbonate precipitation and reverse weathering once river water reaches the ocean, the CO_2 removed from the atmosphere/soil system in the long-term (>1 Ma) is much smaller than the CO_2 consumed in the short-term and according to our calculations amounts to 2.01×10^4 mol km^{-2} y^{-1} on average. This value is almost certainly a minimum estimate of the total amount of CO_2 fixed by weathering on the long-term because in our calculations we assumed that all the alkaline metals deriving from rock weathering in the continents are rapidly involved in the process of reverse weathering in the oceans, while there are still large uncertainties on the magnitude and significance of this process. The values of CO_2 flux consumed by weathering are strongly correlated with runoff while other potential controlling factors show only weak correlations or no correlation. Our estimation of the CO_2 consumed by weathering in the Alpine basins is in the same order of magnitude, but higher than the world average and is consistent with previous estimations made in river basins with similar climatic conditio and similar latitudes.

1. Introduction

Carbon is continuously cycled among oceans, atmosphere, ecosystems, and geosphere (Holland, 1978; Berner, 2003; Kump et al., 2009). Considering the time scale of the phenomena, longer or shorter than one million years, it is possible to distinguish the "short-term" carbon cycle and the "long-term" carbon cycle. In the "short-term" carbon cycle, carbon is exchanged mainly within the superficial systems (atmosphere, oceans, biota, soil, and anthropogenic CO_2 production). Over the "long-term", carbon is involved in slow exchanges between the solid Earth and the ocean–atmosphere system, and the concentration of atmospheric carbon dioxide derives primarily from the balance between CO_2 uptake by chemical weathering and CO_2 release by magmatism–metamorphism (Berner et al., 1983; Berner, 1991, 1994; Berner and Kothavala, 2001; Berner, 2004, 2006; Gislason and Oelkers, 2011; Li and Elderfield, 2013).

Chemical weathering is a key process for understanding the global carbon cycle, both on long and short-terms (Brady, 1991; Kump et al., 2000; White, 2003; Kump et al., 2009; Tipper et al., 2006), and chemical weathering rates are complex functions of many factors including dissolution kinetics of minerals (Brantley, 2003), mechanical erosion (Pinet and Souriau, 1988), lithology (Basu, 1981; Amiotte-Suchet and Probst, 1993a; Amiotte-Suchet and Probst, 1993b; Bluth and Kump, 1994), tectonics (Hren et al., 2007; Dixon et al., 2012; Li et al., 2009), biota (Knoll and James, 1987; Schwartzman and Volk, 1989; Drever, 1994; Berner

* Corresponding author at: CNR-IRPI, Via Madonna Alta, 126, CAP 06128 Perugia, Italy.
E-mail address: marco.donnini@irpi.cnr.it (M. Donnini).

et al., 2003), climate (Fournier, 1960; Walker et al., 1981; Bluth and Kump, 1994), hydrology (Tardy, 1986; Berner and Berner, 1987; Amiotte-Suchet and Probst, 1993b; Velbel, 1993), and various human activities (Flintrop et al., 1996; Yang et al., 1996).

Solutes produced by chemical weathering on the continents are carried to the oceans by rivers. Therefore, the composition of river water is a good indicator of chemical weathering processes (Mackenzie and Garrels, 1966; Garrels and Mackenzie, 1971; Meybeck, 1987; Tardy, 1986; Probst, 1992; Gaillardet et al., 1999; Viers et al., 2007; Berner and Berner, 2012), and the flux of solutes is an indirect measure of the transfer of carbon from the atmosphere to the terrestrial rocks. In fact, given that carbonate and silicate weathering needs atmospheric and soil CO_2 to occur, the evaluation of the weathering rates, that is the knowledge of the dissolved loads transported from the continents to the oceans, allows for an indirect estimation of the atmospheric CO_2 consumed by weathering. Under this perspective, the study of the elemental fluxes due to present day chemical weathering is necessary to understand the past and to make reliable models about the future trends of the global carbon cycle (Brady, 1991; Millot et al., 2002; Beaulieu et al., 2012).

The study of chemical weathering is based on two complementary approaches, namely (i) small scale studies of river basins characterized by a single lithology (Amiotte-Suchet and Probst, 1993b; Bluth and Kump, 1994; White and Blum, 1995; Gislason et al., 1996; Louvat and Allègre, 1997), and (ii) global scale studies based on data from large rivers (Berner et al., 1983; Meybeck, 1987, 2003; Probst et al., 1994; Amiotte-Suchet, 1995; Amiotte-Suchet and Probst, 1995; Boeglin and Probst, 1998; Gaillardet et al., 1999; Mortatti and Probst, 2003). Small scale studies can give detailed data on the weathering rates of a specific rock type under a given climate, while large scale studies can provide global data, integrating the contributions of large portions of continental crust and different climatic regions.

Gaillardet et al. (1999), using an inverse modelling approach based on the river water chemistry and Sr isotopic composition, calculated the weathering rates and the fluxes of CO_2 consumed by rock weathering for the basins of the 60 largest rivers of the world, computing a world average CO_2 consumption due to chemical weathering of 246 mol km^{-2} y^{-1}. Three of the rivers considered in Gaillardet et al. (1999) drain the Alpine chain (i.e., Rhine, Rhone, and Po) and are characterized by CO_2 consumption rates two to five times higher than the world average. Considering the variability of rocks and soils that characterizes the region, the Alpine chain can be considered a model location to study the present-day atmospheric CO_2 consumption over a large region.

In this work, we present a detailed study of the dissolved loads transported by the 32 main Alpine rivers, in order to (i) estimate the present-day weathering rates and the related atmospheric and soil CO_2 consumption for the entire Alpine region, (ii) compare our results with the data of earlier works, (iii) evaluate the relative importance of carbonate and silicate weathering both on short and long-term global carbon cycle, and (iv) determine the main environmental and geological parameters controlling the weathering rates and the CO_2 consumption in the Alps.

Starting from the chemical composition of river waters, the amount of CO_2 consumed by rock weathering has been modelled using a multidisciplinary approach based on the MEGA geochemical code (Major Element Geochemical Approach — Amiotte-Suchet, 1995; Amiotte-Suchet and Probst, 1995, 1996), a GIS based hydrologic and geologic study, and an isotopic study.

2. Study area

The Alps (south-Central Europe) are a collisional belt generated by the convergence of the African and European plates and the consequent closure of the ocean basin located in the Mediterranean region during Cretaceous to present (Trümphy, 1960; Frisch, 1979; Tricart, 1984; Haas et al., 1995; Stampfly et al., 2001; Dal Piaz et al., 2003).

The Alps are characterized by an arc shape and extend, west to east, from the Gulf of Genova to Wien (Fig. 1). South of Genova, the Alpine range disappears, as it was fragmented during the Late Neogene by the opening of the Tyrrenian basin. Here the Alps are partially continuous to the Apennine chain. To the east, the former connection between the Alpine and Carpathian belts is buried below the Neogene fill of the Wien and Styria (Pannonian) basin. North of Alps is located the Molasse Basin (a Cenozoic foredeep basin) that extends from France to the eastern border of Austria. Other major Cenozoic basins are the Rhône Graben to the west, and the Po Plain to the south.

According to the direction of tectonic transport, the Alps (Fig. 1) may be subdivided into two belts of different size, age, and geological characteristics (Dal Piaz et al., 2003): (1) the Europe-vergent belt, a thick collisional wedge of Cretaceous–Neogene age, consisting of continental and minor oceanic units radially displaced towards the Molasse foredeep and the European foreland, (2) the Southern Alps, a shallower (non-metamorphic) and younger (Neogene) thrust-and-fold belt displaced to the south (Adria-vergent), which developed within the Alpine hinterland of the Adriatic upper plate, far from the oceanic suture. The Periadriatic Line, a major fault system of Oligocene–Neogene age, separates these belts. The various segments of the Periadriatic Line take various names, from west to east, the Canavese, Insubric, Giudicarie, Pusteral and Gaital lines (Dal Piaz et al., 2003; Schmid et al., 2004).

From a hydrological point of view, the Alps contribute significantly to the total discharge of the major European rivers, most of which have their headwaters in the Alps and transport the Alpine waters to lower-lying areas. The Alps are crucial for water accumulation and water supply, and therefore they are often referred to as a natural "water towers" (Viviroli and Weingartner, 2004).

Water resources in the Alps are stored in glaciers (in the Alps, around 5150 glaciers presently cover about 2909 km^2, approximately 1.5% of the total area of the Alps), lakes, groundwater reservoirs, and soils. The Alps represent an enormous natural water reservoir since precipitation in winter is retained as snow and ice. Considerable quantities of water can be accumulated and released through the summer melting of glaciers and snow, thus providing water during the dry season when precipitation and runoff are often least in the lowlands, and demands are highest. Particularly, this becomes effective in the dry months of late summer, when the Alps play a distinct supportive role with regard to overall discharge. This natural storage mechanism benefits many river systems in Europe, including the four major alpine rivers, the Rhine, the Danube, the Po, and the Rhône.

A comparison between the proportion of discharge that can be expected on the basis of the catchment size and the actual discharge measured demonstrates the hydrological significance of the Alps that, with a mean contribution ranging from 26% (Danube) to 53% (Po) of the total discharge, supply up to 2–6 times more water than might be expected on the basis of the catchment size (Weingartner et al., 2007).

Generally the Alpine rivers have a maximum flow rate in July, and a minimum rate in January. This is because the runoff of Alpine catchments is influenced by glacier melt, snow accumulation, and snowmelt (Gurtz et al., 1999; Verbunt et al., 2003).

3. Materials and methods

3.1. Theoretical background

The dissolved load of streams originates from atmospheric input, pollution, evaporite dissolution, and weathering of carbonate and silicate rocks. The application of mass balance calculations allows for the quantification of the different contributions (Bricker and Jones, 2003). The quantification of the carbonate and silicate components of dissolved load is essential for the evaluation of the atmospheric/soil CO_2 consumed by rock weathering. In fact, the weathering reactions of silicate mineral hydrolysis and dissolution of carbonates consume atmospheric/soil carbon dioxide and produce an increase of alkalinity

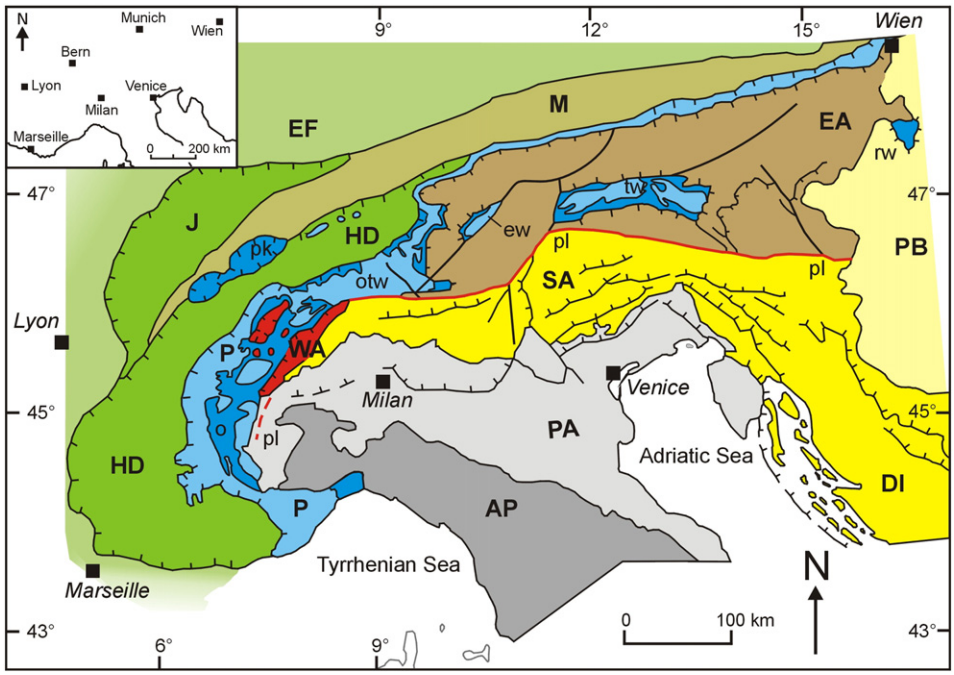

Fig. 1. Location of the study area and tectonic map of Alps (simplified from Dal Piaz et al., 2003). WA = Western Austroalpine; EA = Eastern Austroalpine; P = Penninic domain (continental and ophiolitic (o) nappes in western Alpine arc); HD = Helvetic-Dauphinois domain; M = Molasse foredeep; J = Jura belt. SA = Southern Alps; PB = Pannonian basin; EF = European Foreland; PA = Po Valley and Adriatic foreland; DI = Dinaric thrust-and-fold belt; AP = Apenninic thrust-and-fold belt. otw = Ossola-Ticino tectonic window; ew = Engadine tectonic window; tw = Tauern tectonic window; rw = Rechnitz tectonic window; Pk = Prealpine klippen; pl = periadriatic lineament.

of the solutions (Mortatti and Probst, 2003), as shown by the following reactions:

albite into kaolininite,

$$2NaAlSi_3O_8 + 2CO_2 + 11H_2O \rightarrow Al_2Si_2O_5(OH)_4 + 2HCO_3^- + 2Na^+ + 4H_4SiO_4 \quad (1)$$

K-feldspar into montmorillonite,

$$2KAlSi_3O_8 + 2CO_2 + 6H_2O \rightarrow Al_2Si_4O_{10}(OH)_2 + 2HCO_3^- + 2K^+ + 2H_4SiO_4 \quad (2)$$

Ca-plagioclase into kaolinite,

$$CaAl_2Si_2O_8 + 2CO_2 + 3H_2O \rightarrow Al_2Si_2O_5(OH)_4 + 2HCO_3^- + Ca^{++} \quad (3)$$

olivine weathering,

$$Mg_2SiO_4 + 4CO_2 + 4H_2O \rightarrow 2Mg^{++} + 4HCO_3^- + H_4SiO_4 \quad (4)$$

calcite dissolution,

$$CaCO_3 + CO_2 + H_2O \rightarrow Ca^{++} + 2HCO_3^- \quad (5)$$

dolomite dissolution,

$$CaMg(CO_3)_2 + 2CO_2 + 2H_2O \rightarrow Ca^{++} + Mg^{++}4HCO_3^-. \quad (6)$$

For each process, the moles of atmospheric/soil CO_2 consumed by the weathering of one mole of mineral can be computed from the stoichiometry of the reactions.

Not all the consumed CO_2 is permanently removed from the atmosphere because part of the carbon is returned to the atmosphere through several processes. On time scales longer than 1 Ma, the CO_2 consumed by weathering of carbonates in the continents is returned completely to the atmosphere when carbonate minerals precipitate in the ocean (reverse of reactions (5) and (6)). Half of the CO_2 consumed during weathering of Ca and Mg silicates (reactions (3) and (4)) is precipitated as $CaCO_3$ after transportation of Ca^{++} and HCO_3^- in the ocean, and half is released back into the atmosphere as CO_2 (reverse of reactions (5) and (6)). Finally, the role of Na and K silicates poses some uncertainty. In fact even if their weathering reactions consume CO_2 (reactions (1) and (2)), once the Na^+ and K^+ ions transported by rivers reach the ocean, they may undergo reverse weathering to form authigenic clays and CO_2 (Huh, 2010).

As a result, on the long-term (more than 1 Ma), only weathering of Ca and Mg silicate minerals is a net sink for atmospheric/soil CO_2 (Huh, 2010; Berner et al., 1983), while on shorter time-scales also the alteration of Na and K silicates and the dissolution of Ca and Mg carbonates act as temporary sinks for atmospheric/soil CO_2.

For these reasons, we considered two different mass balance equations. On time-scales shorter than 1 million year (short-term carbon cycle), the total atmospheric/soil CO_2 flux ($F_{CO2\text{-}short}$) consumed by rock weathering on a river basin can be calculated by the following equation:

$$F_{CO2-short} = F_{Na-sil} + F_{K-sil} + 2F_{Mg-sil} + F_{Mg-carb} + 2F_{Ca-sil} + F_{Ca-carb} \quad (7)$$

for time-scales longer than 1 million years (long-term carbon cycle), considering the return of CO_2 to the atmosphere related to carbonate precipitation and reverse weathering, the net flux of CO_2 ($F_{CO2\text{-}long}$) is given by:

$$F_{CO2-long} = F_{Mg-sil} + F_{Ca-sil} \quad (8)$$

where F_X is the flux of a generic chemical species X, given by its molal concentration multiplied by the river flow rate, and the suffixes sil and carb indicate if the considered chemical species derives from silicate or carbonate weathering (for example $F_{Mg\text{-}sil}$ means flux of Mg deriving from silicate weathering). The factor 1 for $F_{Na\text{-}sil}$, $F_{K\text{-}sil}$, $F_{Mg\text{-}carb}$, $F_{Ca\text{-}carb}$ in Eq. (7) and $F_{Mg\text{-}sil}$ $F_{Ca\text{-}sil}$ in Eq. (8) or 2 for $F_{Mg\text{-}sil}$ $F_{Ca\text{-}sil}$ in Eq. (7) derive from the stoichiometric coefficients of the considered weathering reactions (Eqs. (1)-(6)).

Eqs. (7) and (8) are applicable if the following assumptions are valid: (i) carbonic acid is the only source of protons in the weathering reactions (the contribution of other acids like HNO_3, H_2SO_4 is negligible); (ii) the main chemical reactions occurring in the river basins are congruent dissolution of calcite, dolomite and olivine and incongruent dissolution of albite and K-feldspar into kaolinite and of anorthite into montmorillonite; and (iii) pyrite dissolution, producing acidic waters, is negligible.

Further assumptions were considered for the calculation of $F_{CO2\text{-}long}$. These assumptions imply that the value computed with Eq. (8) is just a rough (probably minimum) estimation of the CO_2 permanently removed from the atmosphere. The assumption that all the CO_2 consumed by carbonate dissolution is completely returned to the atmosphere in 1 Ma is widely accepted, and is coherent with the residence time of Ca in the ocean system (1 Ma). In fact, a small part of Ca^{++} from rivers is not removed by carbonate precipitation but is precipitated as anhydrite or gypsum without any CO_2 production (Mackenzie and Garrels, 1966; Emerson and Hedges, 2008), but presently this amount is very small compared to carbonate production, except for very peculiar environments. Larger uncertainties pertain to the role of reverse weathering. This process, by which new clays are formed by chemical combination of elemental material from oceans and marine sediments (Mackenzie and Kump, 1995), has been hypothesised on a thermodynamic basis to explain the apparent imbalance between weathering and marine $CaCO_3$ precipitation in the oceans (Mackenzie and Garrels, 1966; Sillen, 1967), but has little experimental evidence (Emerson and Hedges, 2008). According to Holland (1978), only a small fraction (10–20%) of the clay minerals delivered to the oceans by rivers undergo authigenesis, but recent field and experimental studies (Michalopoulos and Aller, 1995, 2004) have shown that rapid formation of authigenic clay minerals is plausible under certain conditions, and the role of reverse weathering has been revaluated (Li and Elderfield, 2013; Misra and Froelich, 2012). Further sources of uncertainty, could be the role of sulphide oxidation in carbonate dissolution (Torres et al., 2014) and hydrothermal alteration reactions in the ocean.

3.2. Estimation of the CO_2 flux consumed by weathering

For the estimation of the CO_2 flux consumed by weathering in the Alps, we first defined the drainage basins of the main Alpine rivers (Fig. 2) and their hydrologic, geographic, and geologic features (precipitations, mean elevation, drainage basin area, and surface area of the main rock types cropping out in the basin) using a GIS based approach. Next, the selected rivers were sampled near the basin outlets during dry and flood seasons. Then, we applied a revised version of the MEGA (Major Element Geochemical Approach) geochemical code (Amiotte-Suchet, 1995; Amiotte-Suchet and Probst, 1996) to the chemical compositions of the selected rivers in order to discriminate the different components of dissolved load, and to quantify the atmospheric CO_2 consumed by weathering in the Alpine region. The approach was successfully applied to the Congo, Amazon, and Niger River basins (Probst et al., 1994; Boeglin and Probst, 1998; Mortatti and Probst, 2003).

The complete calculation procedure consists of several steps:

First, subtraction of the rain contribution to the river waters composition knowing the X/Cl molal ratios of rainwater in the study area (X = Na, K, Mg, Ca). In this study we applied a further correction subtracting the anthropogenic contribution when it was present. The correction for the anthropogenic contribution is based on the consideration that an excess of Cl with respect to the Na/Cl molal ratio of local meteoric water that generally ranges between 1.0 and 1.1 (Rogora et al., 2006), probably derive from an anthropogenic input. For the few water samples with Cl > Na (Na/Cl < 1.0), the amount of Cl, and consequently all the X/Cl ratios, were corrected assuming Cl = Na.

Second, computation of the dissolved load deriving from silicates dissolution assuming that all Na and K, after the rain correction, derive from silicate weathering. This assumption is acceptable for the purposes of the study since the rain correction implicitly consider also the possible contribution from halite dissolution, a process which leads to a Na/Cl molal ratio in water of 1, just like rainwater.

The amount of Ca and Mg deriving from silicate weathering is computed considering a specific molar ratio, $R_{sil} = (Na + K)/(Ca + Mg)$, for

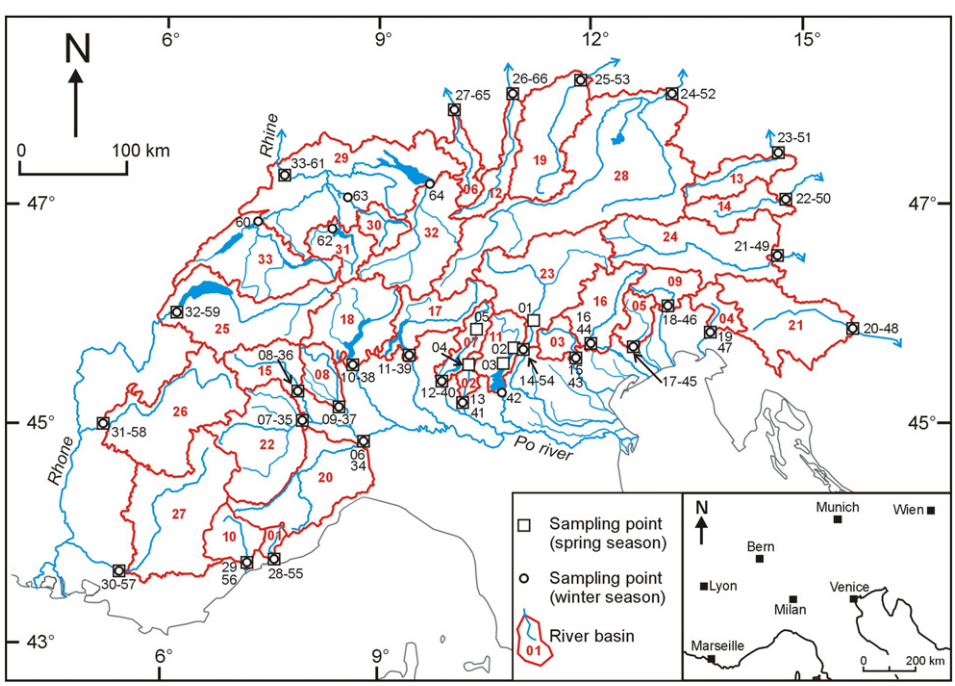

Fig. 2. Selected Alpine drainage basins and location of the sampling points.

each river basin. The average (Na + K)/(Ca + Mg) molal ratio of each basin ($R_{sil\text{-}mean}$) was computed as the weighted average of the R_{sil} values of the various lithologies cropping out in the basin, considering the surface area and the mean precipitation on the surface area of each lithology,

$$R_{sil-mean} = \frac{\sum_{n}^{i=l}(R_{sil-litho-n} \times S_{litho-n} \times P_{litho-n})}{\sum_{n}^{i=l}(S_{litho-n} \times P_{litho-n})} \quad (9)$$

where, $R_{sil\text{-}litho\text{-}n}$ is the (Na + K)/(Ca + Mg) ratio of waters interacting with lithology n, $S_{litho\text{-}n}$ is the surface area covered by the lithology n and $P_{litho\text{-}n}$ is the mean value of precipitation over the outcrops of lithology n.

For the computation of $R_{sil\text{-}mean}$ we built a simplified GIS-based geo-lithological map of the Alps (Fig. 3), giving a specific value of R_{sil} to each lithology according to the literature values estimated from unpolluted French stream waters draining small mono-lithological basins (Meybeck, 1986). Then, we prepared a GIS-based map of the average precipitation on the Alps (Fig. 4a), we established a correlation between terrain elevation and precipitation, and finally we obtained the values of $S_{litho\text{-}n}$ and $P_{litho\text{-}n}$ overlapping the geo-lithological map and the digital elevation model.

Third, estimation of the Ca and Mg amounts originating from carbonate weathering as the remaining cations after the silicate correction:

$$(Ca + Mg)_{carb} = (Ca + Mg)_{river} - (Ca + Mg)_{sil}. \quad (10)$$

For samples showing a clear input of Ca due to gypsum or anhydrite dissolution, we applied a further correction subtracting to $(Ca + Mg)_{carb}$ the moles of Ca deriving from sulphate minerals, that is the excess of SO_4 with respect to the SO_4/Cl molal ratio of local meteoric water.

Forth, multiplication of the molal concentrations of the various components of dissolved load by the river flow rate, and division by the catchment area in order to obtain the elemental flux values (F_X) in mol km^{-2} y^{-1}.

Fifth, computation of the weathering flux, and of the atmospheric/soil CO_2 flux (F_{CO2}) consumed by the rock weathering on short and long-terms using Eqs. (7) and (8).

The procedure was repeated for the spring and the winter seasons.

For the application of the mass balance and for the computation of runoff the following parameters were requested: (i) the daily discharge of each river in the place and at the time of sampling, an information required to transform concentrations to fluxes. These data have been obtained from different sources, including Italian local authorities and Environmental Agencies (ARPA), the Hydrographical Office of Austria, the Federal Office for the Environment in Switzerland, the Environmental Agency of Bavaria, the Meteorological and Hydrological Service of Croatia, and the Ministère de l'Ecologie et du Développement Durable of France. For most catchments, the data were available as flow rates (m^3 s^{-1}), but for some catchments only stage measurements at gauging stations were available. These measurements were converted to discharge estimates using specific rating curves; (ii) the area of each catchment, computable from the available DEM data; (iii) the proportions of the lithological types in each catchment, computable from the available geo-lithological maps of Fig. 3, (iv) the mean precipitation for each basin, computable using an empirical relationship linking terrain elevation to precipitation.

Details on the procedures for the estimation of catchment areas, proportions of lithological types and precipitations are given in Sections 3.3, 3.5 and 3.6 respectively.

3.3. Drainage basins, sampling sites and sampling campaigns

The main Alpine drainage basins were defined from the high-resolution Digital Elevation Model ASTER GDEM (Tachikawa et al., 2011). For each basin, the surface area and the average elevation were computed using GRASS (Neteler and Mitasova, 2008) and QGIS (Quantum GIS Development Team, 2012). After the definition of the drainage basins, we located the sampling stations near the outlet of each basin (Fig. 2, Table 1) and as close as possible to the stations for the measurement of streamflow in order to know the discharge of the river at the time and place of sampling.

The rivers of the study area show average discharge values at the sampling stations ranging from about 100 m^3/s to more than 1300 m^3/s

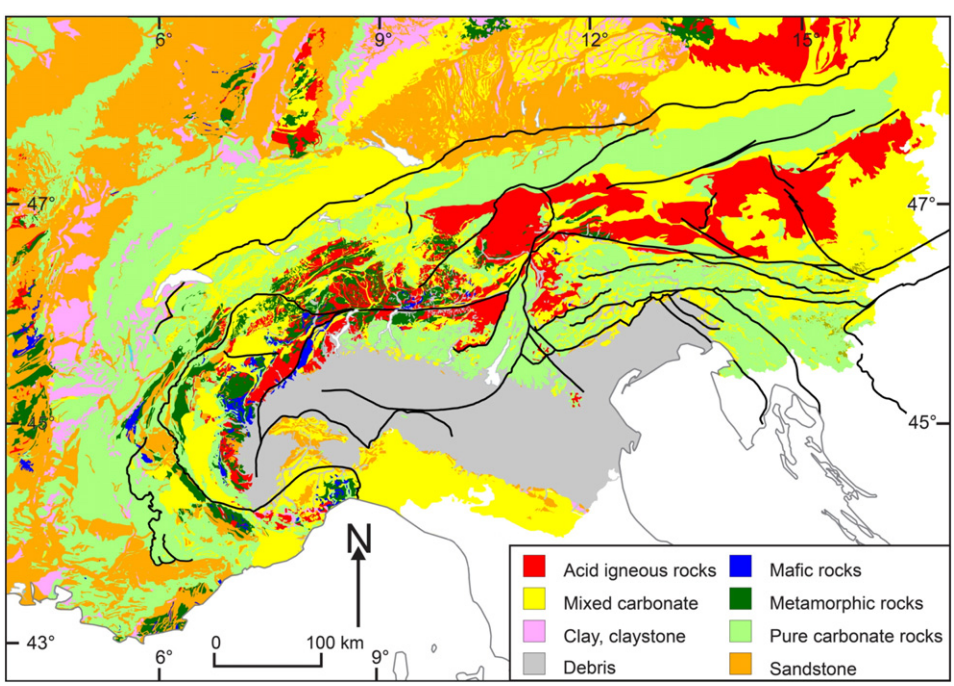

Fig. 3. Geo-lithological map of Alps elaborated according to the lithological classification of Meybeck (1986, 1987).

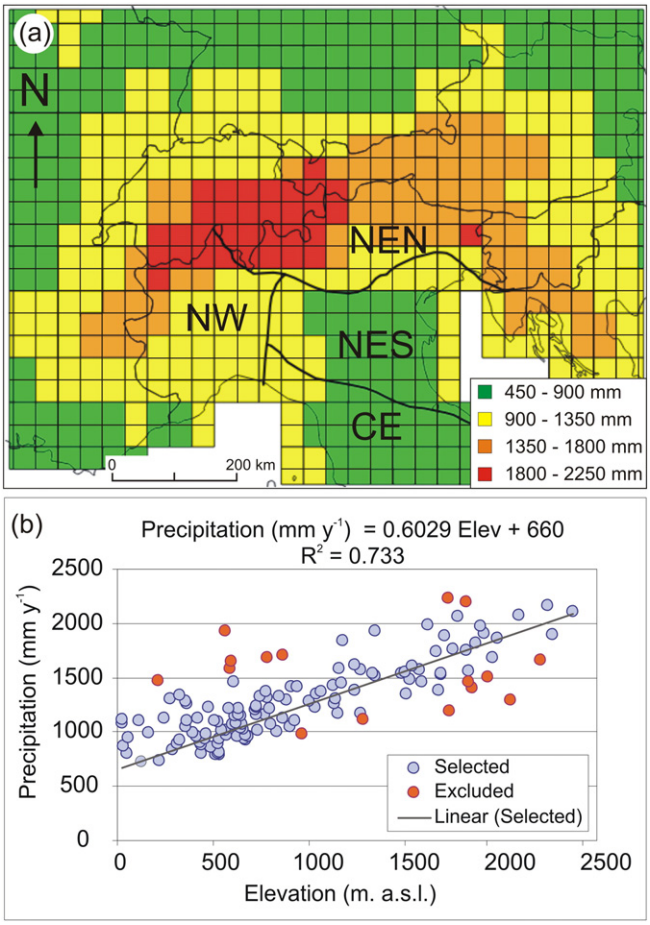

Fig. 4. (a) Mean annual precipitation map for Alpine region elaborated through R software (R Core Team, 2015) starting from the 1961–1990 monthly precipitation (Mitchell and Jones, 2005). The map shows the sub-regions identified by Brunetti et al. (2006): NES (the southern part of north-eastern Italy) with low value of precipitation; CE (central Italy) and NW (north-western Italy) with medium value of precipitation; NEN (northern part of north-eastern Italy) characterized by high values of precipitation. (b) Precipitation vs elevation relationship in Alpine region estimated through the analysis of the distribution of residues method considering the values with residual frequency between 5% and 95%.

(Rhine at Basel). The highest flows occur during spring and summer and the month with the highest flow ranges between June, for hydrological regimes dominated by snow melting, to April, for snowmelt-rainfall mixed regimes (Bard et al., 2015). In particular the rivers of the northern side of the Alpine Chain are dominated by snow-melting and show a maximum discharge in May–June and a minimum in December–February, while the rivers of Southern Alps, affected by precipitation of Mediterranean origin, are generally characterised by a mixed snowmelt–rainfall regime and show a period of maximum discharge in April–May, a minimum in September, a further maximum in November and a minimum in January–February.

In order to sample the river waters during the periods of maximum and minimum discharge, we planned two sampling campaigns. The first campaign was performed from February 2011 to June 2011 (spring season), and the second campaign was executed from December 2001 to March 2012 (winter season). All the samples of the spring campaign have been collected from April 20th to June 21st; same points originally sampled in February 2011 have been re-sampled in April 2011, except for Mincio river that has been sampled two times in February. The winter campaign was originally planned for the period December 2011–February 2012 but some samplings shifted to the first half of March 2012, because the early 2012 European cold wave, characterized intense snowfall and unusually low temperatures.

Table 1
Main features of the studied Alpine basins.

Basin ID	River name	Surface (km^2)	Mean elevation (m asl)	Minimum elevation (m asl)	Maximum elevation (m asl)
01	Roia	663	1244	7	2887
02	Mella	767	510	44	2194
03	Brenta	1601	1112	53	2796
04	Isonzo	1611	828	12	2664
05	Livenza	1770	580	3	2639
06	Iller	2058	916	484	2591
07	Oglio	2099	1234	87	3516
08	Sesia	2298	805	78	4545
09	Tagliamento	2309	1049	105	2728
10	Var	2794	1339	17	3077
11	Mincio	2905	1129	62	3523
12	Lech	2907	1154	431	2956
13	Enns	3179	1346	446	2894
14	Mur	3230	1485	626	3024
15	Dora Baltea	3564	2015	227	4798
16	Piave	4598	1265	74	3273
17	Adda	4707	1565	121	3970
18	Ticino	6614	1292	111	4548
19	Isar	7801	771	381	2940
20	Tanaro	8180	644	45	3204
21	Sava	8337	605	69	2808
22	Po	9058	1078	100	3976
23	Adige	10,197	1675	41	3865
24	Drava	10,492	1381	363	3656
25	Rhône	10,460	1549	305	4777
26	Isere	11,175	1514	112	4023
27	Durance	11,992	1281	169	4037
28	Inn	23,806	1326	305	3991
29	Rhine	36,739	1040	110	4087
30	Linth[a]	1814	1248	185	3605
31	Reuss[a]	2839	1386	205	3592
32	Alpine Rhine[a]	7706	1628	315	3593
33	Aare[a]	8282	1139	359	4080
34	Rhine-Basel[a]	16,098	622	110	2429

[a] Indicates Rhine sub-basins — basin 29 is the sum of basins 30 to 34.

In the first sampling campaign we considered 29 river basins with a maximum area of 36,739 km^2 (Rhine basin), a minimum area of 663 km^2 (Roia basin), and an average catchment area of 6822 km^2. We collected 33 samples, one sample for each basin, and two samples for the Mincio, Adige, Mella and Oglio basins. Three of these samples (01, 04, and 05) were collected upstream of the outlet of the basin (for the Adige, Mella and Oglio basins), whereas for the Mincio basin the two samples were collected at the basin outlet (that coincides with the Garda Lake).

Considering that the Rhine basin is very large when compared to the other Alpine basins and presents a large variability of geologic and climatic conditions, for the second sampling campaign the Rhine basin was further divided into five smaller sub-basins (Linth: 1814 km^2; Reuss: 2839 km^2; Lower Rhine: 7706 km^2; Aare: 8282 km^2; Rhine-Basel: 16,098 km^2). The sum of the areas of the five Rhine sub-basins exactly coincides with the area of the Rhine basin considered in the first campaign. As a result, we obtained 33 basins with an average area of 5933 km^2. During the second campaign we collected 33 samples of river waters, one sample for each drainage basin.

3.4. Sampling and analytical methods

For each sample, temperature, electrical conductivity, pH, Eh, silica, total iron, and alkalinity were measured in the field. Silica and total iron were determined using a colorimetric kit, and alkalinity was determined by acid titration with HCl 0.1 N using methyl orange as indicator. Water samples for chemical analyses were filtered with 0.45 μm filters, and collected in two polyethylene bottles, the first with a volume of 100 mL and the second with a volume of 50 mL. The 50 mL aliquot

was acidified immediately with 0.5 mL of concentrated suprapure HCl in order to stabilize the sample, preventing algal growth and carbonate precipitation. A raw sample for the determination of the isotopic composition of water (δD, $\delta^{18}O$) was collected in the 100 mL polyethylene bottle, and a further aliquot of 250 mL, acidified with 2.5 mL of HNO_3 and stored in a polyethylene bottle previously treated following the indications of Nisi et al. (2008), was collected for the determination of the $^{86}Sr/^{87}Sr$ isotopic ratio.

All the chemical determinations were performed at the Geochemical Laboratory of the Perugia University. Sulphate, NO_3^-, Cl^- and F^- were determined by ion-chromatography. Ca^{++}, Mg^{++}, Sr^{++} concentrations were determined by atomic adsorption (AA) flame spectroscopy on the

Table 2
Location, sampling date and field data of river waters sampled in Alpine region.

Sample number	River	Date	Lat	Long	T (°C)	pH	Eh (mv)	Cond (μS/cm)
01	Adige	9/02/2011	46.14416	11.07477	4.20	8.19	186.00	270
02	Mincio	9/02/2011	45.87467	10.8727	5.60	8.19	131.00	270
03	Mincio	9/02/2011	45.72785	10.71894	8.80	8.65	147.00	240
04	Mella	9/02/2011	45.72385	10.23096	7.70	8.82	92.80	350
05	Oglio	9/02/2011	46.06807	10.35133	5.60	8.51	161.00	160
06	Tanaro	20/04/2011	44.9776	8.77199	15.10	8.07	237.00	475
07	Po	20/04/2011	45.18217	7.88843	16.30	8.13	222.60	339
08	Dora Baltea	20/04/2011	45.46476	7.86924	11.90	8.54	197.20	255
09	Sesia	21/04/2011	45.31634	8.44058	15.60	7.78	223.80	264
10	Ticino	21/04/2011	45.7233	8.6269	13.80	9.08	199.70	165
11	Adda	21/04/2011	45.8224	9.41439	15.50	9.10	190.60	209
12	Oglio	21/04/2011	45.56865	9.85073	15.20	8.84	213.80	300
13	Mella	22/04/2011	45.35568	10.15114	14.60	7.97	209.40	757
14	Adige	22/04/2011	45.86256	10.99878	12.20	8.42	207.50	257
15	Brenta	22/04/2011	45.76467	11.72935	12.40	8.80	218.10	241
16	Piave	22/04/2011	45.90182	11.94685	15.30	8.65	202.60	352
17	Livenza	22/04/2011	45.85054	12.53584	12.60	8.36	243.10	391
18	Tagliamento	23/04/2011	46.23386	13.04341	10.90	8.44	244.80	522
19	Isonzo	23/04/2011	45.95594	13.61318	12.90	8.51	223.70	252
20	Sava	4/05/2011	45.89344	15.60565	18.10	8.85	178.50	372
21	Drava	4/05/2011	46.65578	14.63523	16.30	8.51	210.20	277
22	Mur	5/05/2011	47.19415	14.80768	9.50	8.53	225.30	262
23	Enns	5/05/2011	47.65176	14.75044	8.50	8.27	203.30	246
24	Inn	5/05/2011	48.29419	13.26731	16.40	8.77	209.50	363
25	Isar	6/05/2011	48.46552	11.9461	13.00	8.47	199.10	573
26	Lech	6/05/2011	48.35238	10.93827	14.00	8.47	202.20	396
27	Iller	6/05/2011	48.21117	10.08225	14.30	8.36	179.60	456
28	Roia	20/06/2011	43.82735	7.58289	15.40	8.39	143.00	417
29	Var	20/06/2011	43.78644	7.21318	18.30	8.27	156.00	425
30	Durance	20/06/2011	43.66742	5.49637	21.80	8.19	135.90	520
31	Isere	21/06/2011	45.08493	5.18328	16.10	8.08	134.80	355
32	Rhone	21/06/2011	46.20422	6.14981	13.00	8.21	150.10	295
33	Rhine	21/06/2011	47.55529	7.60364	17.70	8.16	139.00	323
34	Tanaro	5/12/2011	44.9776	8.77199	8.00	8.07	121.10	530
35	Po	5/12/2011	45.18217	7.88843	10.90	7.64	144.40	340
36	Dora Baltea	5/12/2011	45.46476	7.86924	6.60	8.21	227.80	301
37	Sesia	5/12/2011	45.31634	8.44058	10.20	8.13	172.90	333
38	Ticino	6/12/2011	45.7233	8.6269	9.60	7.64	234.60	157
39	Adda	6/12/2011	45.8224	9.41439	11.00	7.83	191.30	184
40	Oglio	6/12/2011	45.56865	9.85073	10.40	8.23	191.00	266
41	Mella	6/12/2011	45.35568	10.15114	10.80	8.00	217.00	730
42	Mincio	6/12/2011	45.44484	10.69411	11.90	8.46	228.40	230
43	Brenta	7/12/2011	45.76467	11.72935	6.40	8.29	239.50	272
44	Piave	7/12/2011	45.90182	11.94685	8.60	8.28	188.30	365
45	Livenza	7/12/2011	45.85054	12.53584	8.30	8.19	207.30	370
46	Tagliamento	7/12/2011	46.23552	13.04348	12.60	7.82	242.40	472
47	Isonzo	8/12/2011	45.95594	13.61318	7.20	8.24	189.00	268
48	Sava	8/12/2011	45.89344	15.60565	11.20	8.29	115.50	388
49	Drava	8/12/2011	46.65578	14.63523	3.40	8.15	169.80	322
50	Mur	9/12/2011	47.19415	14.80768	2.10	8.14	277.80	308
51	Enns	9/12/2011	47.65176	14.75044	3.00	8.23	215.20	332
52	Inn	9/12/2011	48.29419	13.26731	5.40	8.16	216.50	391
53	Isar	9/12/2011	48.46552	11.9461	8.40	8.30	197.80	579
54	Adige	10/12/2011	45.86256	10.99878	5.00	8.29	137.70	301
55	Roia	12/03/2012	43.8153	7.59058	10.70	8.44	142.30	621
56	Var	12/03/2012	43.7721	7.21285	10.10	8.31	137.80	643
57	Durance	12/03/2012	43.6663	5.49444	11.10	8.44	186.40	526
58	Isere	13/03/2012	45.08493	5.18328	8.10	8.15	157.00	577
59	Rhone	13/03/2012	46.20977	6.16694	7.80	8.31	139.70	304
60	Aare	14/03/2012	47.12334	7.23137	5.10	8.18	183.50	379
61	Rhine	14/03/2012	47.55678	7.60082	8.60	8.48	140.60	387
62	Reuss	14/03/2012	47.04597	8.32246	8.80	8.56	185.90	225
63	Linth	15/03/2012	47.35893	8.53721	6.10	8.30	214.30	296
64	Alpine Rhine	15/03/2012	47.49888	9.70219	5.10	8.45	208.80	315
65	Iller	15/03/2012	48.2112	10.08225	7.60	8.19	192.00	509
66	Lech	15/03/2012	48.35235	10.93812	8.00	8.39	nd	436

acidified sample, whereas Na^+, K^+, Li^+ and Rb^+ were determined by atomic emission (AE) flame spectroscopy. The detection limits are: 0.01 mg/L for Ca^{++}, Mg^{++}, Na^+, K^+, F^-, $NO3^-$, Sr^{++}; 0.03 mg/L for Cl^- and $SO4^-$; and 0.01 μg/l for Li^+ and Rb^+. All the laboratory analytical methods and the field alkalinity determinations have an accuracy better than 2%. The total analytical error, evaluated checking the charge balance, is about 2.5% on average, and is lower than 2% for 44% of the samples.

Table 3
Chemical and isotopic composition of river waters sampled in Alpine region.

ID	Ca	Mg	Na	K	Sr	Li	Rb	HCO_3	SO_4	Cl	NO_3	F	$\delta^{18}O$	δD	$^{87}Sr/^{86}Sr$
	(mg/L)	(mg/L)	(mg/L)	(mg/L)	(mg/L)	(μg/L)	(μg/L)	(mg/L)	(mg/L)	(mg/L)	(mg/L)	(mg/L)	(‰ vs V-SMOW)	(‰ vs V-SMOW)	
01	32.40	10.06	4.12	3.17	0.17	4.14	2.4	125.86	17.06	5.41	5.60	0.06	−11.92	−85.1	0.710980
02	38.00	9.14	5.23	2.06	0.14	1.95	2.1	144.52	7.17	6.62	8.37	0.04	−11.00	−75.1	0.709697
03	30.80	7.50	4.42	1.21	0.14	3.05	<1.7	122.29	10.59	5.63	0.89	0.06	−7.63	−55.1	0.708583
04	46.70	10.39	3.52	1.89	0.66	5.81	<1.7	159.62	36.35	4.94	3.44	0.08	−9.39	−61.6	0.708366
05	16.00	4.47	4.62	2.99	0.10	1.88	<1.7	59.70	14.83	3.31	4.32	0.06	−11.05	−72.5	0.720819
06	59.90	10.48	13.97	1.85	0.48	5.18	2.6	172.94	53.15	20.46	11.23	0.11	−11.47	−78.7	0.709166
07	38.00	8.91	10.83	4.75	0.35	2.26	2.5	115.70	37.17	14.94	12.83	0.06	−11.51	−80.2	0.709421
08	34.10	4.84	4.40	2.36	0.37	3.80	2.5	89.62	38.45	6.23	2.37	0.06	−13.7	−98.1	0.709383
09	26.40	6.07	9.95	3.00	0.20	1.17	2.7	85.78	27.49	13.37	7.67	0.10	−10.36	−72.0	0.709836
10	19.95	3.13	3.47	1.63	0.21	1.11	3.6	51.61	26.80	3.56	3.48	0.07	−10.30	−66.9	0.708819
11	25.10	5.67	3.58	2.68	0.21	1.84	3.0	83.59	24.33	4.27	3.14	0.08	−10.32	−68.9	0.710039
12	40.35	6.87	4.25	1.40	0.51	1.95	<1.7	118.77	42.10	4.76	3.55	0.08	−9.71	−67.2	0.708671
13	96.50	10.53	22.43	4.34	0.52	3.43	2.6	301.95	53.03	35.08	27.45	0.14	−8.31	−56.5	0.708557
14	31.28	7.14	5.20	2.28	0.21	4.14	3.0	107.33	29.85	6.33	2.87	0.09	−12.03	−86.0	0.710404
15	33.13	6.69	2.39	0.69	0.07	1.23	<1.7	124.07	13.77	2.72	3.49	0.06	−10.85	−70.6	0.709200
16	47.95	10.27	3.14	0.83	0.29	2.07	1.9	170.33	33.66	3.19	3.78	0.07	−9.96	−64.0	0.707802
17	55.00	10.17	3.01	1.27	0.34	2.14	2.1	188.03	35.18	3.44	6.06	0.07	−9.78	−65.9	0.707987
18	77.90	10.12	2.65	0.56	1.25	3.01	2.3	109.25	141.06	2.57	2.77	0.14	−9.55	−64.4	0.707736
19	35.85	7.39	10.76	0.36	0.05	7.78	<1.7	160.74	5.40	1.68	2.30	0.03	−9.11	−57.4	0.708168
20	49.73	12.72	6.43	0.75	0.11	1.64	2.2	196.13	13.98	7.82	4.41	0.09	−9.39	−63.6	0.708653
21	34.05	8.04	5.00	0.85	0.23	2.67	2.3	122.98	23.19	5.48	2.67	0.12	−11.54	−80.5	0.709909
22	24.90	4.74	17.52	2.46	0.10	2.22	9.7	94.15	34.60	3.95	1.28	0.07	−12.34	−86.8	0.710915
23	31.13	7.00	2.81	0.41	0.15	1.31	<1.7	112.00	19.96	3.61	2.50	0.08	−12.58	−88.3	0.709659
24	46.60	10.59	7.65	1.18	0.22	3.09	2.6	169.81	21.62	11.78	5.41	0.12	−12.17	−87.3	0.709247
25	72.20	19.80	15.60	2.02	0.26	2.26	3.5	273.13	19.44	24.73	11.78	0.11	−9.15	−68.6	0.708766
26	50.35	15.08	5.50	1.49	0.40	2.64	<1.7	199.29	23.34	7.42	4.62	0.12	−11.96	−87.8	0.707868
27	61.40	10.96	9.39	3.28	0.45	2.26	3.0	192.97	15.83	19.85	8.31	0.09	−11.33	−81.0	0.707930
28	63.00	9.06	1.95	0.11	1.20	4.44	2.5	101.15	120.56	1.66	0.30	0.10	−10.72	−72.5	0.708181
29	59.00	7.26	7.94	0.41	1.06	8.44	2.2	86.47	112.70	13.34	0.64	0.16	−11.10	−74.6	0.708284
30	68.80	10.65	10.20	0.63	1.19	8.76	<1.7	137.25	95.30	19.53	3.72	0.12	−10.63	−74.2	0.708143
31	51.20	5.67	4.89	0.54	0.73	4.25	2.6	109.80	74.65	9.15	2.80	0.10	−12.41	−87.7	0.708874
32	40.90	4.96	5.42	1.31	0.52	6.77	3.8	95.53	48.58	10.68	2.54	0.13	−12.23	−91.0	nd
33	48.35	5.71	5.92	0.94	0.40	8.26	2.8	148.23	29.32	10.74	5.29	0.10	−11.02	−81	0.708575
34	66.10	10.04	18.35	2.45	0.53	nd	nd	201.76	53.37	22.59	11.54	0.08	−10.62	−76.4	0.709167
35	33.65	8.76	14.62	3.02	0.27	nd	nd	114.74	30.29	16.58	10.74	0.04	−10.68	−74.5	0.709776
36	39.55	6.93	4.73	1.52	0.44	nd	nd	103.21	45.10	5.25	2.86	0.05	−12.80	−93.7	0.709345
37	34.75	8.20	10.20	2.54	0.35	nd	nd	113.09	33.66	12.02	8.77	0.05	−10.77	−74.7	0.709504
38	17.90	3.06	3.02	1.39	0.22	nd	nd	41.18	24.32	2.78	2.86	0.05	−9.66	−67.3	0.708834
39	21.10	5.11	3.12	1.23	0.18	nd	nd	77.41	20.25	2.68	2.95	0.05	−10.28	−71.8	0.710743
40	34.25	6.67	3.51	1.36	0.48	nd	nd	101.02	31.81	3.58	3.40	0.05	−9.72	−68.7	0.708803
41	88.60	9.37	24.60	3.76	0.60	nd	nd	292.07	44.49	33.00	26.41	0.09	−8.45	−58.5	0.708543
42	28.65	7.85	4.15	1.14	0.14	nd	nd	116.39	9.77	5.48	1.38	0.04	−7.37	−55.9	0.708626
43	36.20	7.98	2.18	0.72	0.11	nd	nd	163.05	14.98	2.40	3.96	0.06	−9.76	−68.9	0.708959
44	46.20	9.29	3.40	1.25	0.18	nd	nd	204.78	14.99	3.51	5.63	0.04	−8.83	−60.7	0.707842
45	50.70	9.29	2.60	0.85	0.35	nd	nd	175.68	31.21	2.53	5.53	0.06	−9.42	−65.2	0.707988
46	61.65	9.28	2.82	0.72	1.04	nd	nd	152.35	92.01	2.44	3.04	0.12	−8.89	−60.1	0.707835
47	37.70	7.63	1.41	0.47	0.07	nd	nd	170.74	4.76	1.78	4.03	0.04	−8.16	−53.3	0.708192
48	49.05	9.31	6.63	1.35	0.16	nd	nd	205.88	15.69	8.16	6.74	0.05	−9.00	−60.0	0.708598
49	36.85	9.32	6.91	1.54	0.28	nd	nd	138.90	27.04	6.56	3.77	0.08	−10.82	−74.0	0.709888
50	32.45	7.00	12.68	2.32	0.16	nd	nd	150.98	29.88	8.87	2.86	0.06	−11.55	−80.5	0.711100
51	37.55	9.40	6.31	1.16	0.27	nd	nd	145.49	30.02	9.47	3.29	0.04	−12.00	−86.7	0.710065
52	46.45	9.44	8.24	2.00	0.29	nd	nd	172.39	24.10	12.51	6.75	0.07	−11.52	−80.6	0.709194
53	68.80	9.47	15.34	3.30	0.25	nd	nd	282.19	20.34	25.25	14.09	0.07	−9.23	−70.0	0.708881
54	33.80	8.85	5.87	2.05	0.27	nd	nd	114.19	36.96	6.64	3.51	0.12	−11.73	−82.2	0.710585
55	101.47	15.31	8.73	0.78	2.17	nd	nd	156.00	186.19	8.00	1.30	0.11	−9.85	−66.0	0.708108
56	97.85	11.06	19.81	1.10	1.76	nd	nd	154.80	160.43	22.53	1.61	0.20	−9.71	−67.7	0.708189
57	70.80	9.05	18.16	0.96	0.93	nd	nd	200.70	56.35	23.16	4.79	0.10	−9.23	−66.3	0.708042
58	81.50	8.91	13.79	0.95	1.34	nd	nd	162.90	106.18	17.17	5.34	0.10	−11.66	−84.5	0.708677
59	42.30	4.53	6.91	2.21	0.54	nd	nd	110.70	40.12	9.42	2.34	0.11	−12.15	−89.1	0.708741
60	57.50	4.95	6.86	1.28	0.45	nd	nd	164.70	23.86	9.10	6.59	0.08	−10.21	−73.3	0.708102
61	52.40	6.05	10.25	1.31	0.44	nd	nd	169.20	24.60	12.29	6.52	0.11	−10.67	−77.5	0.708437
62	36.90	2.57	2.58	0.74	0.29	nd	nd	110.70	12.68	2.39	3.15	0.08	−11.66	−87.3	0.708249
63	44.40	4.53	5.25	1.66	0.35	nd	nd	148.50	12.84	5.76	2.82	0.11	−10.95	−74.9	0.709032
64	51.10	4.46	3.41	0.56	0.34	nd	nd	182.70	7.22	4.02	3.51	0.07	−11.6	−82.2	0.707872
65	70.10	10.56	12.33	1.36	0.43	nd	nd	247.50	11.72	22.73	10.11	0.08	−10.79	−80.8	0.708002
66	57.75	13.64	7.24	0.86	0.45	nd	nd	219.60	22.76	8.57	6.06	0.11	−11.39	−79.6	0.707873

nd = not detected.

The Sr isotopic analyses were performed by Thermal Ionization Mass Spectrometry (TIMS) at the laboratory of Midi-Pyrénées Observatory (OMP, Toulouse), and the isotopic analysis of ^{18}O and D of water were performed by means of standard mass spectrometry techniques at INGV-OV (Napoli) and CNR-IGG (Pisa). The values of δD ($^{2}H/^{1}H$) and of $\delta^{18}O$ ($^{18}O/^{16}O$) are referred as δ (‰) of the standard V-SMOW (Vienna Standard Mean Ocean Water). Analytical errors are: ±1‰ for δD, ±0.08‰ for $\delta^{18}O$, and less than 1% for the $^{87}Sr/^{86}Sr$ ratio. The physical parameters and the results of the chemical and isotopic analysis of river waters are summarized in Tables 2 and 3.

3.5. GIS-based geo-lithological map of Alps

Exploiting published maps in digital formats, we assembled a GIS-based, high resolution (1:1,000,000), geo-lithological map using GRASS (Neteler and Mitasova, 2008) and QGIS (Quantum GIS Development Team, 2012). The data were taken from (i) the Geological Map of Italy at 1:1,000,000 scale (http://www.isprambiente.gov.it), (ii) the Geological Map of Switzerland at 1:500,000 scale (http://www.swisstopo.admin.ch), (iii) the Geological Map of France at 1:1,000,000 scale, (iv) the Geological Map of Slovenia at 1:250,000 scale, obtained from the European Geological Metadata Catalogue (http://one.geology.cz/), (v) the Geological Map of Germany at 1:1,000,000 scale (BGR, 2011), (vi) the Geological Map of Austria at 1:2,000,000 scale (Egger et al., 1999), (vi) the Tectonic Map of the Alps (Schmid et al., 2004) at 1:500,000 scale, and (vii) the Geological Map of the Alps (Garzanti et al., 2010).

As highlighted by Amiotte-Suchet et al. (2003), one of the most important points for the study of the fluxes of matter from rock and soils to rivers and oceans is the presence of carbonate minerals. For this reason, in our map we first divided the carbonate rocks from the silicate rocks. The carbonate rocks were further subdivided in: (1) pure carbonate rocks (dolostone, limestone) and (2) mixed carbonate rocks (marls and other rocks with <50% of carbonate). Silicate rocks, according to Meybeck (1987), were subdivided in: (3) acid igneous rocks, (4) mafic rocks, (5) clay and claystones, and (6) sand and sandstones. The remaining formations were subdivided in (7) generic metamorphic rocks, (8) debris, (9) mud, and (10) peat. The subdivision between "acid rocks" and "mafic rocks" was done according to the QAPF (IUGS, 1973) and TAS (Le Bas et al., 1986) diagrams.

Since for the application of Eq. (9) it is necessary to know the chemical composition of the outcropping rocks, we classified metamorphic rocks according to the chemistry of protolytes (for example, a metaquartzite was considered a sandstone, and a marble a pure carbonate rock). Where data on protolytes were unavailable or unclear, we attributed the metamorphic lithologies to the generic class (7).

The results (Table 4) show that the most abundant rock types are "carbonate rocks", covering 48.13% of the study area (27.69% of pure carbonate rocks, and 20.44% of mixed carbonate rocks) followed by "sand and sandstones" (20.34%), and acid igneous rocks (14.25%).

Table 4
Relative abundance of outcropping rocks in the drainage area of the 32 river basins considered in this work, according to the geo-lithological map of the Alps of Fig. 3.

Rock type	% Area
Pure carbonate rocks	27.69
Mixed carbonate rocks	20.44
Sand, sandstones	20.34
Acid igneous rocks	14.25
Metamorphic rocks	6.76
Debris	6.48
Clay, claystones	1.54
Mafic rocks	1.22
Other rock types	1.27

In the geo-lithological map (Fig. 3) the areas characterized by carbonate rocks encompass the Jura Mountains located in the northwestern Alps, predominantly between France and Switzerland, the Northern Calcareous Alps located north of the Periadriatic Line in Austria and south-eastern Germany and the south-eastern Calcareous Alps located in Italy, Slovenia and partly in Austria.

Mixed carbonate rocks are mainly present in the Molasse Basin, a Cenozoic foredeep basin that extends from France to the eastern border of Austria, with repeated alternations of shallow marine and freshwater deposits (Dal Piaz et al., 2003).

Silicate rocks crop out mainly in the inner core of the Alps where the main crystalline complexes are located, including the Argentera Massif, the Mont Blanc, the Gran Paradiso, the Sesia zone, the Lepontine Alps, the Saint Gotthard, the Oztal complex, and the Australpine Crystalline complexes.

It is interesting to compare the distribution of the rock types in the study area with the world average lithologies. Recently, a new high-resolution global lithological map (GLiM) was assembled from existing regional geological maps (Hartmann and Moosdorf, 2012). According to the GLiM, the continents are covered by 64% sediments (a third of which are carbonates), 13% metamorphics, 7% plutonics, 6% volcanics, and 10% is water or ice. If we exclude from the computation the 10% of the continents that are covered by water and ice, it results that about 71% of the outcropping rocks belong to sedimentary formations (24% carbonates and 47% sand and sandstones, clay or mixed sedimentary formations) and about 29% are igneous or metamorphic rocks. This data basically confirm the previous estimations of Amiotte-Suchet et al. (2003) and indicate that the lithology of the Alpine area roughly approximates the world lithological distribution with a slight overestimation of sedimentary rocks, and a small underestimation of igneous and metamorphic rocks (Table 4).

3.6. Distribution of precipitations in the Alpine region

To use Eq. (9), information on the precipitation for each rock type in each basin is required. We obtained this information by interpolating 1961–1990 average monthly precipitation measurements (Mitchell and Jones, 2005).

Visual inspection of the mean annual precipitation map for the Alps (Fig. 4a) reveals an arc-shaped zone corresponding to the Alpine chain, characterized by high values of precipitation, with the highest precipitation values in the eastern sector of Italian Alps (Friuli-Venezia Giulia) and in central Alps. The obtained mean annual precipitation map was overlapped to the ASTER GDEM (Tachikawa et al., 2011) and then for each cell of the mean annual precipitation map we estimated the mean elevation form the digital elevation model. The linear correlation between precipitation (mm y^{-1}) and terrain elevation (m) was estimated using a robust fitting approach. 17 of 176 points were excluded and considered outlier, because their residual from a linear fitting model were outside the 5th and 95th percentile range. From the linear fitting of the final subset of 159 values we obtained the following equation:

$$\text{Precipitation} = 0.6029\ (\text{mm y}^{-1}) \times \text{Elevation (m)} + 660 \qquad (11)$$

with a coefficient of determination $R^2 = 0.733$ (Fig. 4b).

Table 5 shows for the linear coefficients the estimated values, the associated standard error (Std. Error), the t value and the p values (R Core

Table 5
Results of the linear regression (R Core Team, 2015) of precipitation (mm y^{-1}) and terrain elevation (m) data the in Alpine region.

	Estimated value	Std. error	T value	P value
Intercept	660	27.88	23.68	2×10^{-16}
Angular coefficient	0.6029	0.029	20.76	2×10^{-16}

Team, 2015). As shown by the p values in the table, both the coefficient estimated are significant.

4. Results

4.1. Chemical and isotopic composition of river waters

In the diagram $\delta^{18}O$ vs δD, the samples of the Alpine rivers (Fig. 5) are close to the global meteoric water line (Craig, 1961), show a marked altitude effect and don't show any evident isotopic shift due to evaporation (in the studied rivers runoff prevail over evaporation). Furthermore there is no evident mixing trend with deep thermal water (in the Alps many thermal springs are present but their contribution to total river discharge is negligible).All the samples are below the meteoric water line of the Mediterranean area (IAEA, 1981; Longinelli and Selmo, 2003), indicating that the largest part of precipitations in the Alps derive from weather fronts originating in the Atlantic ocean or in the Eurasian continent.

The investigated waters were in the range 2.1 °C–21.8 °C, had pH values from 7.64 to 9.10, and exhibited positive Eh values (>100 mV). Total dissolved solids (TDS) varied between 96 and 551 mg/L and, on average, were slightly higher for samples taken in the winter campaign (mean of spring campaign TDS = 253 ± 89 mg/L; mean of winter campaign TDS = 283 ± 101 mg/L). This variation is probably related to the dilution effect related to snow melting during the spring and the relative higher contribution of groundwater during winter.

The Langelier–Ludwig diagram (Fig. 6) shows that most of the waters are characterized by a bicarbonate earth-alkaline composition. Some samples show a clear trend towards a sulphate composition, and other samples a slight enrichment in alkaline metals. The prevalent bicarbonate earth-alkaline composition is due to the dissolution of carbonates that are present in all the considered catchments. The sulphate enrichment that characterizes the rivers from SE France, Roia, Var, Isere and Durance (Olivier et al., 2009) and the Tagliamento River in the SE Italian Alps (Stefanini, 1976), is likely to depend primarily on the interaction with gypsum layers that are present within the Triassic carbonate sequences present in the areas. The slight increase in alkaline metals observed in some samples is due to the incongruent dissolution of silicate minerals, which are ubiquitous in all the studied catchments.

The presence of different sources of solutes is shown by the $^{87}Sr/^{86}Sr$ versus Sr/Na diagram (Fig. 7) that compares the composition of sampled waters with three end-members, namely carbonate rocks, evaporates, and acid-silicate rocks, and with the average rainwater composition. Visual inspection of the diagram reveals that nearly all the samples plot between the carbonate and the evaporite end-members. A trend towards the acid silicate rocks end-member is also apparent. These observations are in good agreement with the distribution of the rock types in the study area (Table 4), and suggest that the sampled waters are a

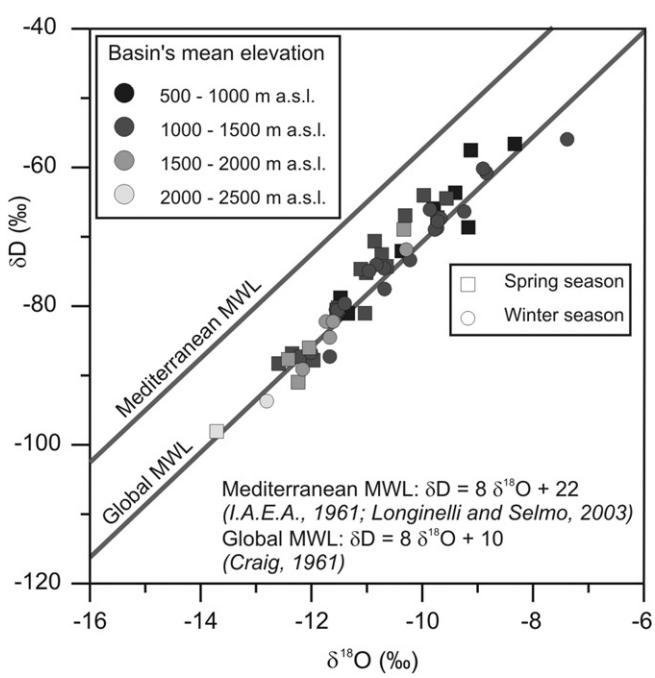

Fig. 5. δD Vs $\delta^{18}O$ for the sampled river waters. The mean elevation of each basins and the sampling season are highlighted.

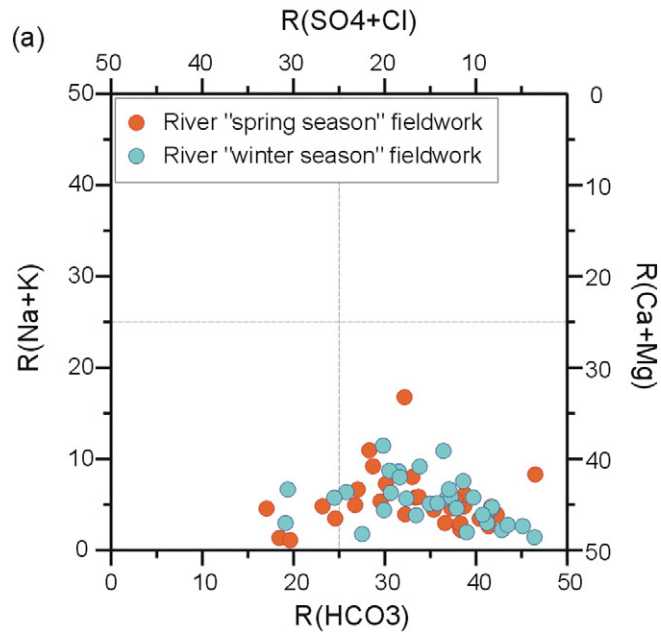

Fig. 6. Langelier–Ludwig diagram for the sampled river waters.

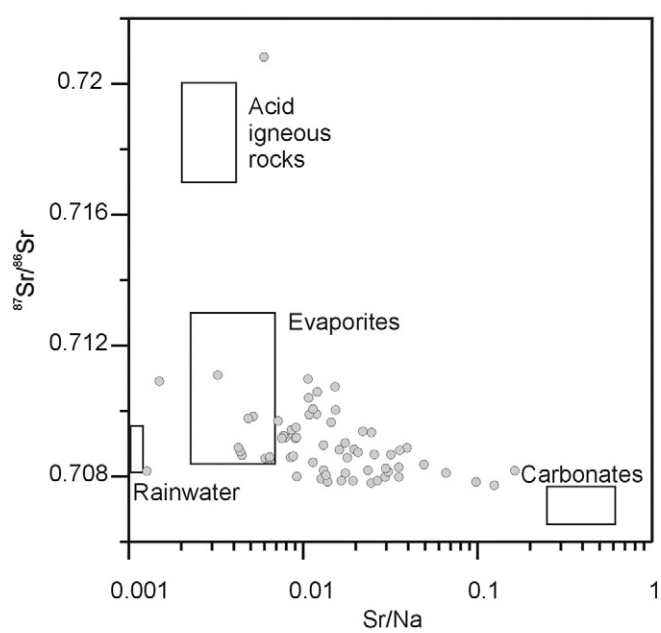

Fig. 7. $^{87}Sr/^{86}Sr$ Vs Sr/Na molar ratio for the sampled river waters. The carbonate and silicate end members are taken from pristine French monolithological stream data (corrected for atmospheric inputs) published by Meybeck (1986), the rain water end member is taken from Roy et al. (1999), and the evaporite end member is based on two headwater samples of the Chang Jiang Tibetan river (Noh et al., 2009).

highly representative of the water-rock interactions in the Alpine catchments.

4.2. Representativity of the geochemical dataset

The chemical composition of each sample analysed in this work represent the composition of a specific river at the date of sampling. In order to check the representativity of our dataset, our analyses have been compared to the available literature data. Considering that Eqs. (7) and (8) used for the computation of the fluxes request the concentrations of Ca, Mg, Na, and K, the concentrations of major cations analysed in this study have been compared to the mean values and standard deviations, σ, of literature data for the following rivers: Adige, Rhone, Rhine, Tagliamento, Livenza, Po, Isonzo and Ticino (Fig. 8 — Stefanini, 1976; Mosello et al., 2001; C.N.R.-I.S.E. Sezione di Idrobiologia ed Ecologia delle Acque Interne, 2004; C.N.R.-I.S.E. Sede di Verbania, 2007; Peripoli, 2008; Olivier et al., 2009; Uehlinger et al., 2009; C.N.R.-I.S.E. Sede di Verbania, 2013; Marchina et al., 2014; unpublished data from Università degli Studi di Perugia, Dipartimento di Fisica e Geologia, Perugia, Italy).

The diagrams of Fig. 8 clearly show that almost all of our data fall in the $\pm 1\sigma$ interval (they are all comprised in the $\pm 2\sigma$ interval) and the average values of the two campaigns are very close to the mean values of literature data (differences are limited to few concentration units).

On average the differences (in %) between the mean concentrations of our data and the mean values obtained from literature data are: 3.9% for Ca, 13.3% for Mg, 20.8% for Na and 5% for K. The average standard deviation are: $\sigma Ca = 18.7\%$, $\sigma Mg = 24.1\%$, $\sigma Na = 40.8\%$ and $\sigma K = 33.1\%$. These values have been used for the computation of the uncertainty on the CO_2 fluxes computed with Eqs. (7) and (8).

4.3. Solute fluxes, weathering rates, and CO_2 fluxes

For each basin, we computed (i) the flux of dissolved solids, expressed as the annual dissolved yield and given by the product of TDS concentration by runoff, (ii) the weathering rate, calculated from the difference between the dissolved solids in the stream outflow and atmospherically/biologically derived components (assuming chloride to be conservative) multiplied by runoff, and (iii) the total atmospheric/soil CO_2 flux consumed by rock weathering, calculated following the procedure described in Section 3.2.

The results of the mass balance calculations, listed in Table 6, reveal variable values of the solute flux, weathering rate, and CO_2 flux. The solute flux ranges from 8×10^3 to 411×10^3 kg km^{-2} y^{-1}, with an average of $127 \times 10^3 \pm 29 \times 10^3$ kg km^{-2} y^{-1}. It is strongly correlated with $F_{CO2\text{-short}}$, but shows a weak correlation with $F_{CO2\text{-long}}$ (Fig. 9). The weathering rate ranges from 3×10^3 to 339×10^3 kg km^{-2} y^{-1},

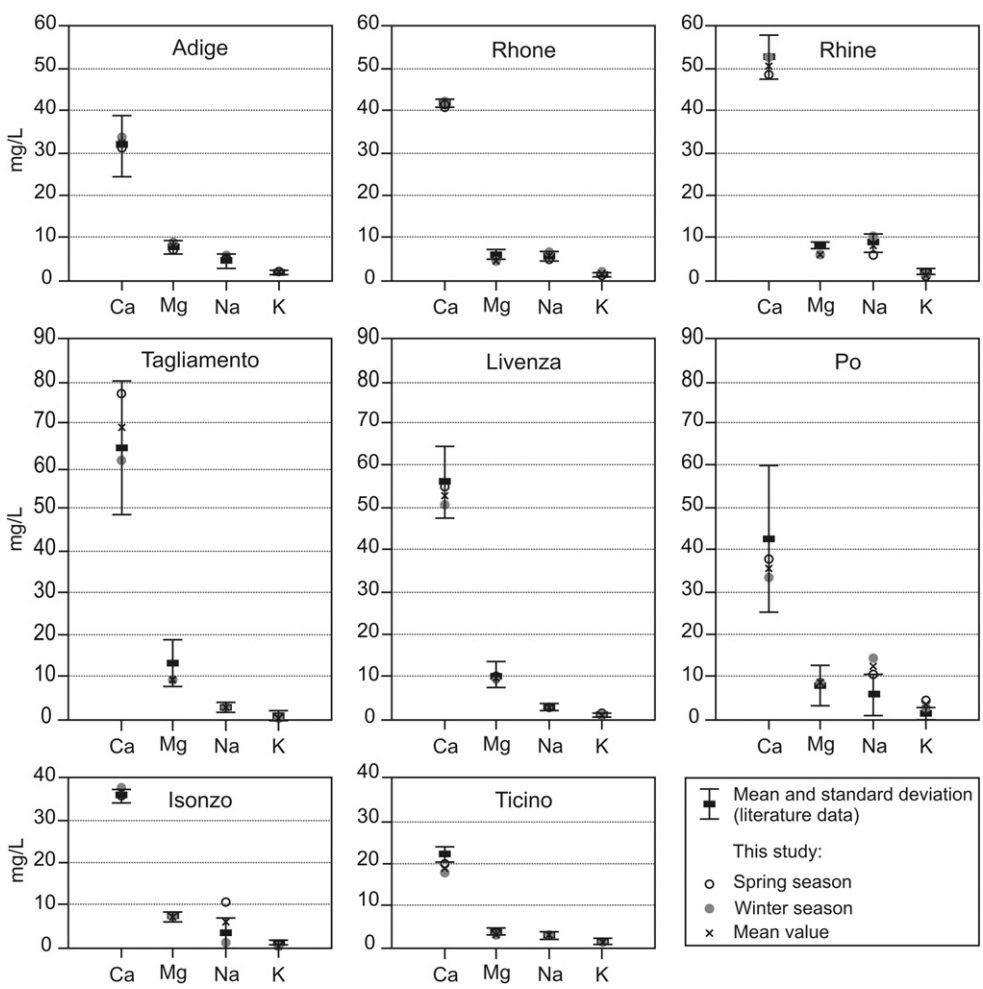

Fig. 8. Comparison of Ca, Mg, Na and K of our samples of Rhine, Rhone, Adige, Po, Ticino, Tagliamento, Livenza and Isonzo with data from literature. The mean and standard deviation values are compared to data from this study. Rhine data refer to the period 1995–2004 (Uehlinger et al., 2009), Rhone data refer to the period 1985–2004 (Olivier et al., 2009), Adige data consist of 15 samples collected in 2008 (Peripoli, 2008), Po data consist of 9 samples collected in 2012 (Marchina et al., 2014), Ticino data consist of 41 samples from 1998 to 2012 (Mosello et al., 2001; C.N.R.-I.S.E. Sezione di Idrobiologia ed Ecologia delle Acque Interne, 2004; C.N.R.-I.S.E. Sede di Verbania, 2007; C.N.R.-I.S.E. Sede di Verbania, 2013; unpublished data from Università degli Studi di Perugia, Dipartimento di Fisica e Geologia, Perugia, Italy).

Table 6
Summary of results: $F_{(Ca+Mg)sil}$, $F_{(Ca+Mg)carb}$, $F_{(Na+K)sil}$ are respectively the flux of (Ca + Mg) deriving from silicate weathering, the flux of (Ca + Mg) deriving from carbonate weathering and the flux of (Na + K) deriving from silicate weathering. $F_{CO2\text{-}short}$ and $F_{CO2\text{-}long}$ are the fluxes of atmospheric CO_2 consumed by chemical weathering considering, respectively, the short term and the long term carbon cycle. In the same table are also reported the values of flow rate, runoff, solute flux and chemical weathering.

Basin ID and name	Water sample	Season	$F_{(Ca+Mg)sil}$	$F_{(Ca+Mg)carb}$	$F_{(Na+K)sil}$	$F_{CO2\text{-}short}$	$F_{CO2\text{-}long}$	Flow rate	Runoff	Solute flux	Chemical weathering rate
			mol y^{-1} km^{-1}	mol y^{-1} km^{-1}	mol y^{-1} km^{-1}	mol y^{-1} km^{-1}	mol y^{-1} km^{-1}	m^3 s^{-1}	l s^{-1} km^{-1}	t km^{-2} y^{-1}	t km^{-2} y^{-1}
01 — Roia	28	Spring	1.35×10^4	5.74×10^5	1.10×10^4	6.12×10^5	1.35×10^4	6.67	10.06	95	92
02 — Mella	13	Spring	1.77×10^3	1.50×10^5	4.84×10^3	1.58×10^5	1.77×10^3	3.35	4.37	76	24
03 — Brenta	15	Spring	7.36×10^3	8.29×10^5	1.93×10^4	8.63×10^5	7.36×10^3	44.70	27.92	165	131
04 — Isonzo	19	Spring	0.00	9.08×10^5	0.00	9.08×10^5	0.00	42.00	26.07	185	140
05 — Livenza	17	Spring	3.92×10^4	2.13×10^6	3.68×10^4	2.25×10^6	3.92×10^4	76.30	43.11	411	339
06 — Iller	27	Spring	4.40×10^3	3.40×10^5	4.04×10^3	3.53×10^5	4.40×10^3	17.93	8.71	88	54
07 — Oglio	12	Spring	6.42×10^3	4.16×10^5	1.70×10^4	4.46×10^5	6.42×10^3	27.49	13.10	92	68
08 - Sesia	09	Spring	1.44×10^4	8.18×104	1.74×10^4	1.28×10^5	1.44×10^4	43.51	18.93	107	17
09 — Tagliamento	18	Spring	8.22×10^3	6.12×10^5	1.05×10^4	6.39×10^5	8.22×10^3	20.51	8.88	97	98
10 — Var	29	Spring	4.49×10^3	3.75×10^5	4.09×10^3	3.88×10^5	4.49×10^3	29.10	10.42	95	59
11 — Mincio	02	Spring	5.69×10^2	5.32×10^4	1.55×10^3	5.59×10^4	5.69×10^2	5.19	1.79	12	8
11 — Mincio	03	Spring	4.55×10^2	4.21×10^4	1.24×10^3	4.43×10^4	4.55×10^2	5.15	1.77	10	7
12 — Lech	26	Spring	1.15×10^4	9.91×10^5	1.06×10^4	1.02×10^6	1.15×10^4	63.20	21.74	211	156
13 — Enns	23	Spring	3.96×10^3	6.97×10^5	1.08×10^4	7.16×10^5	3.96×10^3	81.96	25.78	146	110
14 — Mur	22	Spring	1.05×10^5	1.52×10^5	2.88×10^5	6.49×10^5	1.05×10^5	44.10	13.65	79	76
15 — Dora Baltea	08	Spring	2.99×10^3	4.02×10^5	4.93×10^3	4.13×10^5	2.99×10^3	64.60	18.13	104	63
16 — Piave	16	Spring	9.47×10^3	4.10×10^5	1.17×10^4	4.40×10^5	9.47×10^3	42.44	9.23	80	66
17 — Adda	11	Spring	2.16×10^4	4.39×10^5	4.03×10^4	5.22×10^5	2.16×10^4	110.80	23.54	113	76
18 — Ticino	10	Spring	4.63×10^4	4.59×10^5	6.03×10^4	6.12×10^5	4.63×10^4	248.00	37.50	134	87
19 — Isar	25	Spring	5.20×10^3	2.61×10^5	4.63×10^3	2.76×10^5	5.20×10^3	46.80	6.00	83	42
20 — Tanaro	06	Spring	1.38×10^4	3.79×10^5	1.02×10^4	4.16×10^5	1.38×10^4	121.00	14.79	161	62
21 — Sava	20	Spring	1.83×10^4	5.12×10^5	1.74×10^4	5.66×10^5	1.83×10^4	105.74	12.68	117	84
22 — Po	07	Spring	6.96×10^3	1.27×10^5	5.64×10^3	1.47×10^5	6.96×10^3	80.30	8.87	68	21
23 — Adige	14	Spring	7.75×10^3	3.46×10^5	1.72×10^4	3.78×10^5	7.75×10^3	158.77	15.57	94	57
24 — Drava	21	Spring	6.31×10^3	2.83×10^5	1.73×10^4	3.13×10^5	6.31×10^3	110.17	10.50	67	47
25 — Rhone	32	Spring	5.63×10^3	5.59×10^5	5.97×10^3	5.76×10^5	5.63×10^3	233.00	22.28	148	88
26 — Isere	31	Spring	1.70×10^4	1.19×10^6	8.16×10^3	1.23×10^6	1.70×10^4	377.06	33.74	275	188
27 — Durance	30	Spring	4.81×10^2	3.27×10^4	3.89×10^2	3.41×10^4	4.81×10^2	9.26	0.77	8	5
28 — Inn	24	Spring	3.93×10^3	5.95×10^5	7.15×10^3	6.10×10^5	3.93×10^3	450.21	18.91	164	93
29 — Rhine	33	Spring	2.98×10^3	4.72×10^5	4.49×10^3	4.83×10^5	2.98×10^3	564.00	15.35	123	74
01 — Roia	55	Winter	2.74×10^4	4.09×10^5	2.22×10^4	4.86×10^5	2.74×10^4	3.38	5.10	77	73
02 — Mella	41	Winter	8.70×10^3	2.33×10^5	2.38×10^4	2.74×10^5	8.70×10^3	7.80	10.17	168	40
03 — Brenta	43	Winter	7.16×10^3	9.06×10^5	1.88×10^4	9.39×10^5	7.16×10^3	42.30	26.39	193	143
04 — Isonzo	47	Winter	0.00	1.65×10^6	0.00	1.65×10^6	0.00	73.10	45.38	327	254
05 — Livenza	45	Winter	2.25×10^4	8.46×10^5	2.11×10^4	9.12×10^5	2.25×10^4	32.40	18.31	161	137
06 — Iller	65	Winter	0.00	6.66×10^5	0.00	6.66×10^5	0.00	36.50	17.74	216	103
07 — Oglio	40	Winter	1.18×10^4	6.31×10^5	3.13×10^4	6.86×10^5	1.18×10^4	46.05	21.94	128	103
08 — Sesia	37	Winter	6.70×10^3	4.67×10^4	8.11×10^3	6.82×10^4	6.70×10^3	7.30	3.18	22	9
09 — Tagliamento	46	Winter	3.85×10^4	1.76×10^6	4.93×10^4	1.88×10^6	3.85×10^4	73.72	31.93	327	287
10 — Var	56	Winter	4.53×10^4	3.26×10^5	4.12×10^4	4.58×10^5	4.53×10^4	20.10	7.19	106	64
11 — Mincio	42	Winter	2.93×10^2	3.85×10^4	8.00×10^2	3.99×10^4	2.93×10^2	4.89	1.68	9	6
12 — Lech	66	Winter	7.43×10^4	1.78×10^6	6.83×10^4	1.99×10^6	7.43×10^4	112.00	38.53	409	293
13 — Enns	51	Winter	1.32×10^3	3.04×10^5	3.62×10^3	3.10×10^5	1.32×10^3	36.88	11.60	89	48
14 — Mur	50	Winter	2.61×10^4	1.25×10^5	7.15×10^4	2.49×10^5	2.61×10^4	25.80	7.99	62	32
15 — Dora Baltea	36	Winter	1.07×10^4	3.55×10^5	1.77×10^4	3.94×10^5	1.07×10^4	42.30	11.87	78	59
16 — Piave	44	Winter	6.02×10^3	2.32×10^5	7.46×10^3	2.52×10^5	6.02×10^3	25.96	5.65	51	38
17 — Adda	39	Winter	3.17×10^4	5.40×10^5	5.90×10^4	6.63×10^5	3.17×10^4	145.60	30.93	131	96
18 — Ticino	38	Winter	3.82×10^4	3.30×10^5	4.97×10^4	4.56×10^5	3.82×10^4	185.00	27.97	85	64
19 — Isar	53	Winter	3.55×10^3	1.17×10^5	3.16×10^3	1.27×10^5	3.55×10^3	32.50	4.17	58	19
20 — Tanaro	34	Winter	3.70×10^4	1.51×10^5	2.74×10^4	2.53×10^5	3.70×10^4	61.00	7.46	91	32
21 — Sava	48	Winter	1.60×10^4	3.98×10^5	1.52×10^4	4.45×10^5	1.60×10^4	95.03	11.40	109	65
22 — Po	35	Winter	3.43×10^4	2.17×10^4	2.78×10^4	1.18×10^5	3.43×10^4	58.90	6.50	48	11
23 — Adige	54	Winter	7.87×10^3	2.58×10^5	1.75×10^4	2.91×10^5	7.87×10^3	102.68	10.07	67	43
24 — Drava	49	Winter	7.46×10^3	1.79×10^5	2.05×10^4	2.15×10^5	7.46×10^3	66.38	6.33	46	31
25 — Rhone	59	Winter	1.53×10^4	7.03×10^5	1.62×10^4	7.49×10^5	1.53×10^4	333.00	31.84	220	112
26 — Isere	58	Winter	1.02×10^5	7.64×10^5	4.90×10^4	1.02×10^6	1.02×10^5	212.95	19.06	238	140
27 — Durance	57	Winter	2.42×10^3	1.58×10^4	1.96×10^3	2.26×10^4	2.42×10^3	8.20	0.68	8	3
28 — Inn	52	Winter	2.06×10^3	2.61×10^5	3.74×10^3	2.69×10^5	2.06×10^3	218.73	9.19	82	41
29 — Rhine	61	Winter	3.01×10^4	4.98×10^5	4.55×10^4	6.04×10^5	3.01×10^4	708.00	19.27	172	87
30 — Linth	63	Winter	2.27×10^4	1.01×10^6	5.80×10^4	1.11×10^6	2.27×10^4	61.18	33.73	240	167
31 — Reuss	62	Winter	1.57×10^4	5.14×10^5	2.39×10^4	5.69×10^5	1.57×10^4	53.40	18.81	102	84
32 — Alpine Rhine	64	Winter	5.50×10^2	4.75×10^4	1.06×10^3	4.96×10^4	5.50×10^2	9.51	1.23	10	8
33 — Aare	60	Winter	7.21×10^3	7.49×10^5	1.59×10^4	7.79×10^5	7.21×10^3	175.77	21.22	184	119
34 — Rhine-Basel	[a]	Winter	5.90×10^4	5.24×10^5	8.44×10^4	7.29×10^5	5.90×10^4	408.14	25.35	248	99.9

[a] For the computation of the fluxes of sub-basin 34, has been used the composition of sample 61 after subtraction of the mean, weighted on discharge, of samples 60, 62, 63 and 64.

with an average of $83 \times 10^3 \pm 16 \times 10^3$ kg km^{-2} y^{-1}, and is always lower than the solute flux, because the latter comprises the atmospheric and biologic components.

During the "spring season" the fluxes of CO_2 consumed by rock weathering ($F_{CO2\text{-}short}$) ranges form 2.60×10^4 mol km^{-2} y^{-1} (Durance) to 2.03×10^6 mol km^{-2} y^{-1} (Livenza), with an average of

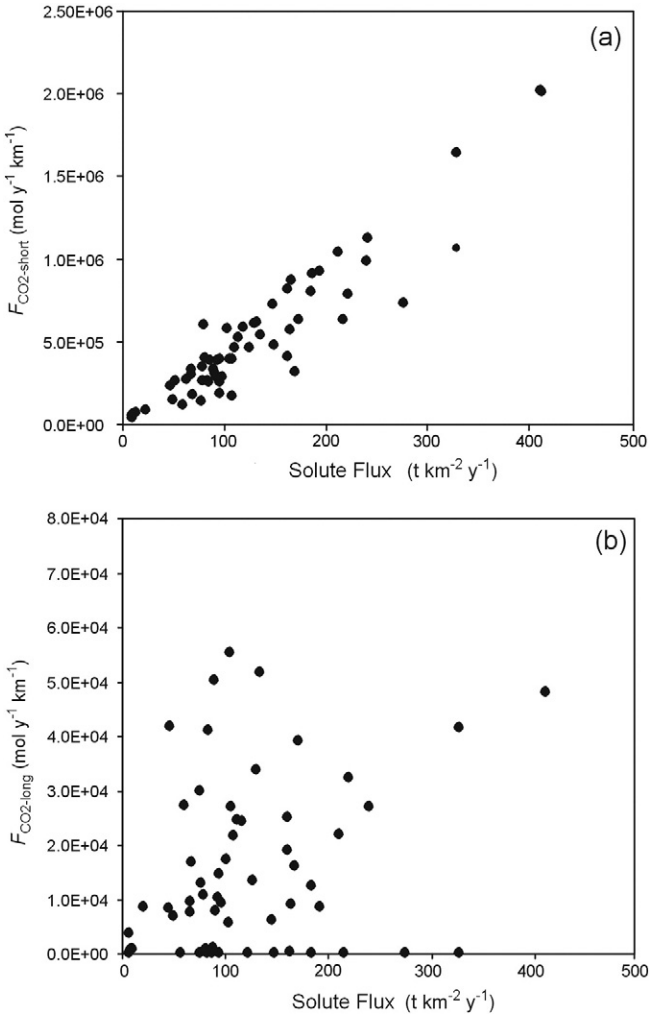

Fig. 9. Comparison between flux of solute flux and F_{CO2} considering (a) the short-term carbon cycle and (b) the long-term carbon cycle.

$4.69 \times 10^5 \pm 1.03 \times 10^5$ mol km^{-2} y^{-1}, whereas in the "winter season" they range from 2.48×10^4 (Durance) to 2.04×10^6 mol km^{-2} y^{-1} (Lech), with an average of $5.35 \times 10^5 \pm 0.97 \times 10^5$ mol km^{-2} y^{-1}. The average value of $F_{CO2\text{-short}}$ considering all the measurements is $5.03 \times 10^5 \pm 1.00 \times 10^5$ mol km^{-2} y^{-1}, and the total amount of CO_2 consumed by short-term weathering is $9.42 \times 10^{10} \pm 1.88 \times 10^{10}$ mol y^{-1}.

If we consider the long-term carbon cycle, the net amount of atmospheric CO_2 fixed by weathering is more than one order of magnitude lower, with a mean value of $F_{CO2\text{-long}} = 2.01 \times 10^4 \pm 0.41 \times 10^4$ mol km^{-2} y^{-1}, and a total amount of CO_2 fixed of by long-term weathering of $4.03 \times 10^9 \pm 0.79 \times 10^9$ mol y^{-1}. The estimated long-term CO_2 fluxes show a very large variability from basin to basin and range form 0.00 mol km^{-2} y^{-1} (Rhein, Rhone, Isere, Durance, Var, Iller, Isar, Isonzo and Mella) to 1.06×10^5 mol km^{-2} y^{-1} (Mur), with an average value of $1.43 \times 10^4 \pm 0.30 \times 10^4$ mol km^{-2} y^{-1}, during the "spring season", while during the "winter season" it varies from 0.00 mol km^{-2} y^{-1} (Isonzo, Isar and Iller) to 1.45×10^5 mol km^{-2} y^{-1} (Isere), with an average value of $2.54 \times 10^4 \pm 0.51 \times 10^4$ mol m^{-2} y^{-1}.

5. Discussion

For most of the considered basins, the CO_2 consumed by weathering is slightly higher in the winter than in the spring, but the variations are limited. Conversely, the differences observed comparing different basins are large, with the values of $F_{CO2\text{-short}}$ ranging over two orders of magnitude, and the values of $F_{CO2\text{-long}}$ ranging over five orders of magnitude.

The comparison between the $F_{CO2\text{-long}}$ and the $F_{CO2\text{-short}}$ values indicates that the CO_2 removed from the atmosphere/soil system in the long-term (>1 Ma) is significantly smaller than the CO_2 consumed by weathering in the short-term. On average, $F_{CO2\text{-long}}$ is 4.8% of $F_{CO2\text{-short}}$. This indicates that >95% of the CO_2 consumed by chemical weathering is returned to the atmosphere within 1 Ma. However, it is necessary to consider that the assumptions made for the calculation of $F_{CO2\text{-long}}$ give a minimum estimate for the long-term atmospheric CO_2 removal.

To search for relationships between F_{CO2} (both in the short and in the long-term) and the potential controlling factors, we considered the variables runoff, precipitation, temperature, elevation, and lithology, and we searched for possible correlations between the variables calculating the sample Pearson product–moment correlation coefficient (r) and the Spearman's rank correlation coefficient (r_s) for each pair of variables (Pearson, 1895; Spearman, 1904). Results are listed in Table 7. $F_{CO2\text{-short}}$ is characterized by a strong correlation with runoff ($r = 0.857$; $r_s = 0.883$), no significant correlations with precipitation, temperature and elevation, a weak positive correlation with the percentage of carbonate rocks cropping out in the basin, and a weak negative correlation with the percentage of silicates. $F_{CO2\text{-long}}$ exhibits a moderate correlation with runoff ($r = 0.415$; $r_s = 0.436$), no correlation with precipitation, temperature and elevation, weak correlations with the lithological types i.e., negative correlations with carbonates, and positive correlations with silicates. Fig. 10 shows the correlation between F_{CO2} and Runoff considering (a) the short-term carbon cycle and (b) the long-term carbon cycle.

To search for a functional relation linking the controlling factors and the F_{CO2} values, we performed a multiple regression analysis considering as independent (explanatory) variables only the potential controlling factors that in the correlation analysis showed some degree of correlation with the CO_2 flux (Table 7), that is runoff and the percentages of carbonates, Na-K silicates, and Ca-Mg silicates. We obtained two regression equations, for the short-term and the long-term CO_2 flux. The equations are

$$F_{CO2-short} = 3143.75 \times X_1 + 336.71 \times X_2 - 5608.00 \times X_3 + 2335.76 \times X_4 + 37,182.96, \quad (12)$$

with a rss $= 2.7 \times 10^{12}$, and

$$F_{CO2-long} = 71.85 \times X_1 - 31.22 \times X_2 + 284.18 \times X_3 + 153.29 \times X_4 - 2293.10, \quad (13)$$

with a rss $= 2.41 \times 10^{10}$,where $F_{CO2\text{-short}}$ and $F_{CO2\text{-long}}$ are the CO_2 fluxes in mol km^{-2} y^{-1}, X_1 is runoff in l s^{-1} km^{-1}, X_2, X_3 and X_4 are the percentages of carbonates, Na–K silicates, and Ca–Mg silicates cropping out in each basin, respectively, while rss is the regression sum of square.

The results of the multiple regression modelling reveals a very good correlation between the values of $F_{CO2\text{-short}}$ computed from the multiple regression on controlling factors and the values derived from the application of the geochemical model (Fig. 11a). This suggests that in the Alps the main factor controlling the CO_2 consumption is runoff, and to a lesser extent lithology. The average value of $F_{CO2\text{-short}}$ obtained by the regression model (4.93×10^5 mol km^{-2} y^{-1}) is very close to value obtained by the geochemical model (5.03×10^5 mol km^{-2} y^{-1}), and it's a further confirmation of the reliability of our data, considering that the two models are based on two independent sets of runoff data. The clear correlation between $F_{CO2\text{-short}}$ and runoff is in a good agreement with Kump et al. (2000), and indicates an important dependence of chemical erosion rates and CO_2 fluxes on the intensity of the hydrological cycle.

On the contrary, as expected from the correlation analysis, the values of $F_{CO2\text{-long}}$ obtained by the regression model do not correlate well with the values obtained by the geochemical model (Fig. 11b).

Table 7
Correlations between F_{CO2}, and controlling factors: (a) Pearson product–moment correlation coefficients and (b) Spearman's correlation coefficients.

	$F_{CO2\text{-short}}$	$F_{CO2\text{-long}}$	Runoff	Precipitation	Temperature	Elevation	% carbonate rocks	% Na-K silicates	% Ca-Mg silicates
Pearson correlation matrix									
$F_{CO2\text{-short}}$	1.000	0.415	0.857	0.053	0.069	0.098	0.258	−0.345	−0.151
$F_{CO2\text{-long}}$	0.415	1.000	0.359	0.034	−0.008	−0.139	−0.346	0.335	0.347
Runoff	0.857	0.359	1.000	0.303	−0.115	0.011	0.239	−0.263	−0.190
Precipitation	0.053	0.034	0.303	1.000	−0.805	0.554	0.204	−0.056	−0.312
Temperature	0.069	−0.008	−0.115	−0.805	1.000	−0.659	−0.097	−0.060	0.225
Elevation	0.098	−0.139	0.011	0.554	−0.659	1.000	−0.406	0.508	0.267
% carbonate rocks	0.258	−0.346	0.239	0.204	−0.097	−0.406	1.000	−0.929	−0.944
% Na–K silicates	−0.345	0.335	−0.263	−0.056	−0.060	0.508	−0.929	1.000	0.758
% Ca–Mg silicates	−0.151	0.347	−0.190	−0.312	0.225	0.267	−0.944	0.758	1.000
Spearman correlation matrix									
$F_{CO2\text{-short}}$	1.000	0.436	0.883	0.182	−0.099	−0.032	0.271	−0.321	−0.270
$F_{CO2\text{-long}}$	0.436	1.000	0.384	−0.002	0.189	0.040	−0.182	0.141	0.201
Runoff	0.883	0.384	1.000	0.343	−0.171	0.428	0.267	−0.281	−0.262
Precipitation	0.182	−0.002	0.343	1.000	−0.777	0.587	0.184	−0.054	−0.243
Temperature	−0.099	0.189	−0.171	−0.777	1.000	−0.608	−0.135	0.017	0.208
Elevation	−0.032	0.040	0.428	0.587	−0.608	1.000	−0.425	0.531	0.351
% carbonate rocks	0.271	−0.182	0.267	0.184	−0.135	−0.425	1.000	−0.956	−0.975
% Na–K silicates	−0.321	0.141	−0.281	−0.054	0.017	0.531	−0.956	1.000	0.890
% Ca–Mg silicates	−0.270	0.201	−0.262	−0.243	0.208	0.351	−0.975	0.890	1.000

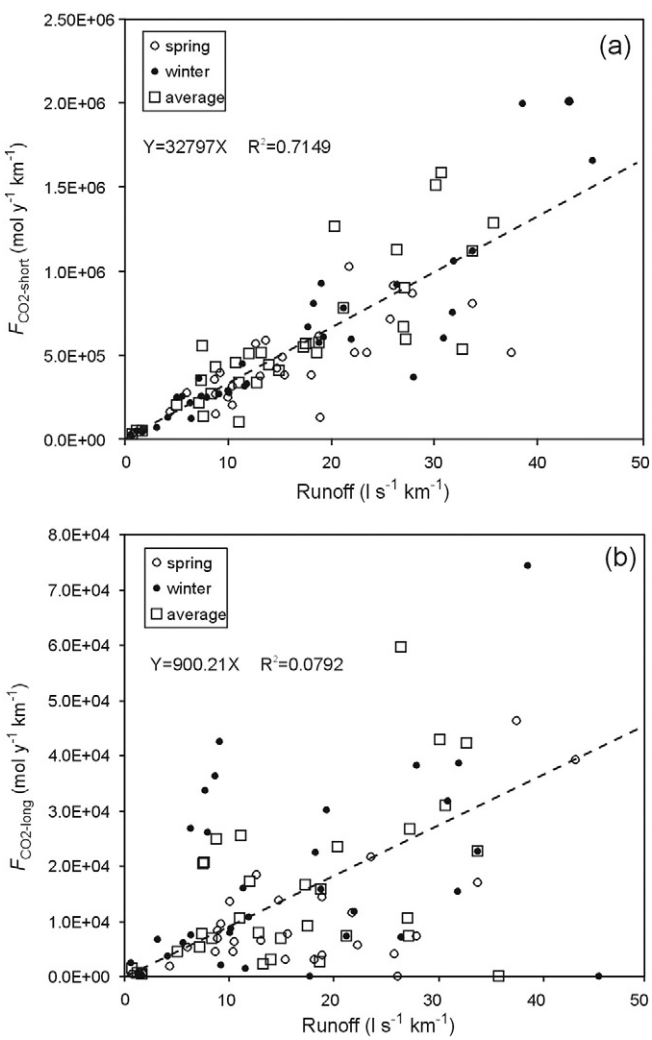

Fig. 10. Correlation between F_{CO2} and Runoff considering (a) the short-term carbon cycle and (b) the long-term carbon cycle. The regression lines are obtained considering intercept = 0.

The average value for the $F_{CO2\text{-long}}$ obtained using the regression model (1.50×10^4 mol km^{-2} y^{-1}) and the geochemical model (2.01×10^4 mol km^{-2} y^{-1}) are similar.

Considering the good correlation of $F_{CO2\text{-short}}$ with the controlling factors, we computed from Eq. (12) the values of the short-term CO_2

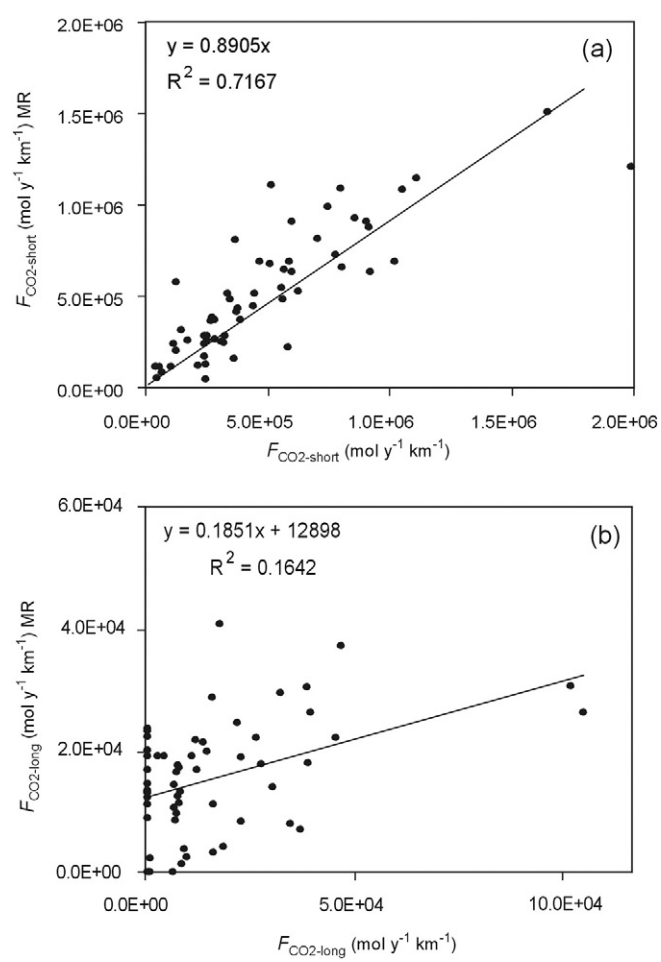

Fig. 11. Comparison between F_{CO2} derived from chemical analyses and F_{CO2} computed through the multiple regression analyses on controlling factors.

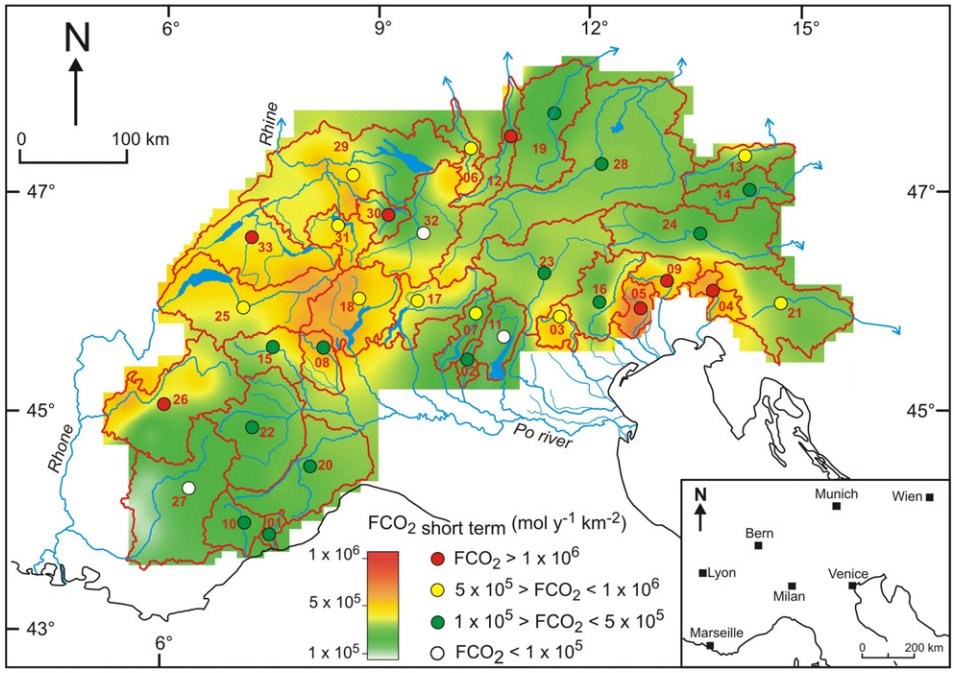

Fig. 12. Map of short-term carbon consumption in the Alps.

flux on a regular 50 km × 50 km grid covering the whole study area (223,613 km^2), basing on average runoff values, and we prepared a map showing the average CO_2 consumption in the Alps (Fig. 12). The map, computed using the Sequential Gaussian Simulation method (Deutsch and Journel, 1988; Cardellini et al., 2003), reveals two areas with high CO_2 consumption rates in the Alps: (i) a large area in the central-western Alps, including the Aare, Reuss, Ticino, and part of the Rhone, Isere, Linth and Rhine River basins, and (ii) an areas in eastern Alps encompassing the Livenza, Isonzo, and Tagliamento River basins. In the same map (Fig. 12), we show the values obtained using the geochemical model. It is noteworthy their good spatial correlation with the $F_{CO2\text{-short}}$ values obtained by the regression model.

6. Conclusions

Estimation of CO_2 consumption in the Alps is a good proxy for present day global CO_2 consumption at mid latitudes, because lithology in the Alps approximates the average composition of the continental crust, and climate in the region is relatively stable compared to other regions at similar latitudes where extreme climatic events are more frequent.

The Alps are characterized by chemical weathering rates ranging over two orders of magnitude, with an average value of $83 \times 10^3 \pm 16 \times 10^3$ kg km^{-2} y^{-1}. Considering the entire region, the chemical weathering process removes from the atmosphere/soil system $9.42 \times 10^{10} \pm 1.88 \times 10^{10}$ mol y^{-1} of CO_2, corresponding to an average CO_2 flux per unit area of $5.03 \times 10^5 \pm 1.00 \times 10^5$ mol km^{-2} y^{-1}. The value is higher, but of the same order of magnitude of the world average CO_2 consumed by weathering (2.46×10^5 mol km^{-2} y^{-1} – Gaillardet et al., 1999), close to the values estimated for the Amazon River (2.71×10^5 mol km^{-2} y^{-1} – Amiotte-Suchet and Probst, 1993a; 3.11×10^5 mol km^{-2} y^{-1} – Probst et al., 1994), and one order of magnitude higher than the estimates for the Congo River (5.05×10^4 mol km^{-2} y^{-1} – Amiotte-Suchet and Probst, 1993b; 5.00×10^4 mol km^{-2} y^{-1} – Probst et al., 1994). Our estimates are consistent with previous estimations in river basins with similar climatic conditions and latitudes, including the Garonne River, where a CO_2 consumption of 2.24×10^5 mo km^{-2} y^{-1} was estimated using a similar approach (Amiotte-Suchet and Probst, 1993a), and a consumption in the range 1.13×10^5 mol km^{-2} y^{-1} (Semhi et al., 1993) to 4.41×10^5 mol km^{-2} y^{-1} (Etchanchu and Probst, 1988) was estimated on the basis of HCO_3^- river fluxes measurements.

Only a small part of the CO_2 removed from the atmosphere/soil system is stored in the solid Earth system for a long-term (>1 Ma). According to our calculations, more than 95% of the CO_2 consumed by chemical weathering is returned to the atmosphere within one million year, and the long-term CO_2 flux ($F_{CO2\text{-long}}$) is about 5% of the short-term CO_2 flux ($F_{CO2\text{-short}}$). However, the $F_{CO2\text{-long}}$ value must be considered just a rough (probably minimum) estimation of the actual value, because it was computed assuming that alkaline metals deriving from rock weathering are rapidly involved in the process of reverse weathering; and there are still large uncertainties on the magnitude and significance of reverse weathering process, carbonate dissolution driven by sulphide oxidation, hydrothermal alteration reactions in the ocean.

Determining what are the most important environmental and/or geologic factors affecting the extent of chemical weathering and CO_2 consumption remains debated. Several works assert the pre-eminence of climatic factors, primarily temperature (e.g., Berner, 1994), but some case studies underscore the primary importance of bedrock lithology and other geologic factors in chemical weathering (e.g., Edmond and Huh, 1997).

In our study, the analysis of the controlling factors exhibits a correlation between $F_{CO2\text{-short}}$ weathering rates and runoff, indicating an important dependence of CO_2 consumption on the intensity of the hydrological cycle, but also an indirect dependence on some geologic factors. In fact, runoff is given by the difference between precipitation, evaporation-transpiration (dependent on temperature), and infiltration, which depends on soil type, thickness, composition, permeability, and the degree of fracturing state of the parent bedrock.

On the contrary, the correlations of $F_{CO2\text{-long}}$ with runoff and other controlling factors were weak or absent, because the main factors affecting $F_{CO2\text{-long}}$ are external to the studied system (carbonate precipitation and eventually reverse weathering occur in the oceans).

The primary role of runoff as weathering controlling factor is in good agreement with previous findings by Amiotte-Suchet and Probst (1993b), (1995) and Kump et al. (2000). Depending both on climatic and geologic variables, runoff acts as a "summing factor",

at least in climatically homogeneous regions like the Alps, and its role in modelling the short-term carbon cycle and climate should be carefully considered.

Acknowledgements

We would like to thank all the people and the institutions that made possible this work and two anonymous reviewers that significantly contributed to the overall quality of the manuscript.

For the laboratory analysis we are grateful to Fausto Matteucci and Gianluca Polidori of the Geochemical Laboratory of Perugia University, to Giovanni Chiodini and Stefano Caliro of the Geochemical Laboratory of Osservatorio Vesuviano — INGV of Napoli, to Marie José Tavella, Jonathan Prunier and Pierre Brunet of the laboratories of Midi-Pyrénées Observatory (OMP — Toulouse) and Ecolab (Laboratoire écologie fonctionnelle et environnement — Toulouse).

For the hydrological data we are grateful to Angela Sulis (ARPA Lombardia), to Alberto Deana, Ivano Di Fant and Andrea Marin (Regione Friuli Venezia Giulia), to Gianmarco Egiatti (ARPA Veneto), to Emanuela Bassi (ARPA Piemonte), to Tomislava Bošnjak (Meteorological and Hydrological Service, Croazia) and to the staff of the Ufficio Dighe Provincia di Trento.

For the fieldworks we are grateful to Keegan Alagna and Angela Baldini (Perugia University) and to Luca Delucchi (Fondazione Edmund Mach — Istituto Agrario di San Michele all'Adige).

References

Amiotte-Suchet, P., 1995. Cycle du carbone, érosion chimique des continents et transfert vers les océans. Sci. Géol. Mém. Strasbourg 97, 156.

Amiotte-Suchet, P., Probst, J.L., 1993a. Modelling of atmospheric CO_2 consumption by chemical weathering of rocks: application to the Garonne, Congo and amazon basins. Chem. Geol. 107, 205–210.

Amiotte-Suchet, P., Probst, J.L., 1993b. Flux de CO_2 consommé par altération chimique continentale: influences du drainage et de la lithologie. C. R. Acad. Sci. Paris II Méc. Phys. Chim. Astron. 317, 615–622.

Amiotte-Suchet, P., Probst, J.L., 1995. A global model for present day atmospheric CO_2 consumption by chemical erosion of continental rocks (GEM CO_2). Tellus 47, 273–280.

Amiotte-Suchet, P., Probst, J.L., 1996. Origines du carbone inorganique dissous dans les eaux de la Garonne: variation saisonnieres et interannuelles. Sci. Géol. Bull. Strasbourg 49, 101–126.

Amiotte-Suchet, P., Probst, J.L., Ludwig, W., 2003. Worldwide distribution of continental rock lithology: implications for the atmospheric/soil CO_2 uptake by continental weathering and alkalinity river transport to the oceans. Glob. Biogeochem. Cycles 17, 1038. http://dx.doi.org/10.1029/2002GB001891.

Bard, A., Renarda, B., Langa, M., Giuntolia, I., Korckc, J., Koboltschnigd, G., Janžae, M., D'Amico, M., Volkeng, D., 2015. Trends in the hydrologic regime of Alpine rivers. J. Hydrol. http://dx.doi.org/10.1016/j.jhydrol.2015.07.052.

Basu, A., 1981. Weathering before the advent of land plants: evidence from unaltered detrital K-felspars in Cambrian–Ordovician arenites. Geology 9, 505–506.

Beaulieu, E., Goddéris, Y., Donnadieu, Y., Labat, D., Roelandt, C., 2012. High sensitivity of the CO_2 sink by continental weathering to the future climate change. Nat. Clim. Chang. 2, 346–349. http://dx.doi.org/10.1038/nclimate1419.

Berner, R.A., 1991. A model for atmospheric CO_2 over Phanerozoic Time. Am. J. Sci. 291, 339–379.

Berner, R.A., 1994. Geocarb II: a revised model of atmospheric CO_2 over Phanerozoic Time. Am. J. Sci. 294, 56–91.

Berner, R.A., 2003. The long-term carbon cycle, fossil fuels and atmospheric composition. Nature 426, 323–326.

Berner, R.A., 2004. The Phanerozoic Carbon Cycle: CO_2 and O_2. Oxford University Press, Oxford.

Berner, R.A., 2006. GEOCARBSULF: a combined model for Phanerozoic atmospheric O_2 and CO_2. Geochim. Cosmochim. Acta 70, 5653–5664. http://dx.doi.org/10.1016/j.gca.2005.11.032.

Berner, E.K., Berner, R.A., 1987. The Global Water Cycle. Geochemistry and Environment. Prentice Hall, Engelwood Cliffs, New Jersey.

Berner, E. K., Berner, R. A., Moulton, K.L., 2003. Plants and Mineral Weathering: Present and Past. In: Drever, J.I., (Ed.) Holland, H.D., Turekian, K.K., (Executive Eds.) Surface and Ground Water, Weathering, and Soils. Treatise on Geochemistry, Volume 5, Elsevier, p.169–188.

Berner, E.K., Berner, R.A., 2012. Global Environment: Water, air, and Geochemical Cycles. second edition. Princeton University Press, Princeton, New Jersey.

Berner, R.A., Lasaga, A.C., Garrels, R.M., 1983. The carbonate-silicate geochemical cycle and its effect on atmospheric carbon dioxide over the past 100 million years. Am. J. Sci. 283, 641–683.

Berner, R.A., Kothavala, Z., 2001. Geocarb III: a revised model of atmospheric CO_2 over Phanerozoic time. Am. J. Sci. 301, 182–204.

Bluth, G.J.S., Kump, L.R., 1994. Lithological and climatological controls of river chemistry. Geochim. Cosmochim. Acta 58, 2341–2359.

Boeglin, J.L., Probst, J.L., 1998. Physical and chemical weathering rates and CO_2 consumption, in a tropical lateritic environment: the upper Niger basin. Chem. Geol. 148, 137–156.

Brady, P.V., 1991. The effect of silicate weathering on global temperature and atmospheric CO_2. J. Geophys. Res. Solid Earth 96 (B11), 18101–18106.

Brantley, S. L., 2003. Reaction kinetics of primary rock-forming minerals under ambient conditions. In: Drever, J.I., Holland, H.D., Turekian, K.K., Surface and ground water, weathering, and soils. treatise on geochemistry, 5, Elsevier, 73–117.

BGR (2011) Geologische Karte der Bundesrepublik Deutschland 1:1,000,000 (GK1000), BGR, Hannover.

Bricker, O.P., Jones, B.F., 2003. Mass-balance approach to interpreting weathering reactions in watershed systems. In: Drever, J.I., Holland, H.D., Turekian, K.K. Surface and Ground Water, Weathering, and Soils. Treatise on Geochemistry, 5, Elsevier, 119–132.

Brunetti, M., Maugeri, M., Monti, F., Nanni, T., 2006. Temperature and precipitation variability in Italy in the last two centuries from homogenised instrumental time sereis. Int. J. Climatol. 26, 345–381.

Cardellini, C., Chiodini, G., Frondini, F., 2003. Application of stochastic simulation to CO_2 flux from soil: mapping and quantification of gas release. J. Geophys. Res. 2425. http://dx.doi.org/10.1029/2002JB002165.

C.N.R.-I.S.E. Sezione di Idrobiologia ed Ecologia delle Acque Interne, 2004I. Ricerche sull'evoluzione del lago Maggiore. Aspetti limnologici. Programma quinquennale 1998–2002. Campagna 2002. Commissione Internazionale per la protezione delle acque italo-svizzere (Ed.: 153 pp. http://www.cipais.org).

C.N.R.-I.S.E. Sede di Verbania, 2007. Ricerche sull'evoluzione del Lago Maggiore. Aspetti limnologici. Programma quinquennale 2003–2007. Campagna 2007 e Rapporto Quinquennale 2003–2007. Commissione Internazionale per la protezione delle acque italo- svizzere (Ed.: 132 pp. http://www.cipais.org).

C.N.R.-I.S.E. Sede di Verbania, 2013. Ricerche sull'evoluzione del Lago Maggiore. Aspetti limnologici. Programma quinquennale 2008–2012. Campagna 2012 e Rapporto Quinquennale. Commissione Internazionale per la protezione delle acque italo-svizzere (Ed.: 133 pp. http://www.cipais.org).

Craig, H., 1961. Isotopic variations in meteoric waters. Science 133, 1702–1703.

Dal Piaz, G.V., Bistacchi, A., Massironi, M., 2003. Geological outline of the Alps. Episodes 26, 175–180.

Deutsch, C.V., Journel, A.G., 1998. GSLIB: Geostatistical Software Library and Users Guide. Applied Geostatistical Series. Oxford University Press, New York.

Dixon, J.L., Hartshorn, A.S., Heimsath, A.M., Di Biase, R.A., Whipple, K.X., 2012. Chemical weathering response to tectonic forcing: a soils perspective from the San Gabriel Mountains, California. Earth Planet. Sci. Lett. 323-324, 40–49. http://dx.doi.org/10.1016/j.epsl.2012.01.010.

Drever, J.I., 1994. The effect of land plants on weathering rates of silicate minerals. Geochim. Cosmochim. Acta 58, 2325–2332.

Edmond, J.M., Huh, Y., 1997. Chemical weathering yields from basement and orogenic terrains in hot and cold climates. In: Ruddiman, W.F. (Ed.), Tectonic Uplift and Climate Change. Plenum Press, New York, pp. 329–351.

Egger, H., Krenmayr, H.G., Mandl, G.W., Matura, A., Nowotny, A., Pascher, G., Pestal, G., Pistotnik, J., Rockenschaub, M., Schnabel, W., 1999. Geological Map of Austria 1: 2.000.000. Geologische Bundesanstalt, Wien, Austria.

Emerson, S.R., Hedges, J.I., 2008. Chemical Oceanography and the Marine Carbon Cycle. Cambridge University Press (462 pp.).

Etchanchu, D., Probst, J.L., 1988. Evolution of the chemical composition of the Garonne river water during the period 1971–1984. Hydrol. Sci. J. 33, 243–256.

Flintrop, C., Hohlmann, B., Jasper, T., Korte, C., Podlaha, O.G., Scheele, S., Veizer, J., 1996. Anatomy of pollution: rivers of North Rhine-Westphalia, Germany. Am. J. Sci. 296, 59–98.

Fournier, F., 1960. Climat et Érosion. Presses Universitaries de France, Paris.

Frisch, R., 1979. Tectonic progradation and plate tectonic evolution of the Alps. Tectonophysics 60, 121–139.

Gaillardet, J., Dupré, B., Louvat, P., Allègre, C.J., 1999. Global silicate weathering and CO_2 consumption rates deduced from the chemistry of large rivers. Chem. Geol. 159, 3–30.

Garrels, R.M., Mackenzie, F.T., 1971. Evolution of Sedimentary Rocks. Norton & Co., New York.

Garzanti, E., Resentini, A., Vezzoli, G., Andò, S., Malusà, M.G., Padoan, M., Paparella, P., 2010. Detrital fingerprint of fossil continental-subduction zones (Axial Belt Provenance, European Alps). J. Geol. 118, 341–362.

Gislason, S.R., Arnorsson, S., Armansson, H., 1996. Chemical weathering of basalt in southwest Iceland: effects of runoff, age of rocks and vegetative/glacial cover. Am. J. Sci. 296, 837–907.

Gislason, S.R., Oelkers, E.H., 2011. Silicate rock weathering and the global carbon cycle. In: Harmon, R., Parker, A. (Eds.), Frontiers in Geochemistry: Contribution of Geochemistry to the Study of the Earth. Wiley-Blackwell (84-103 pp.).

Gurtz, J., Baltensweiler, A., Lang, H., 1999. Spatially distributed hydrotope-based modelling of evapotranspiration and runoff in mountainous basins. Hydrol. Process. 13, 2751–2768.

Haas, J., Kovacs, S., Krystin, L., Lein, R., 1995. Significance of Late Permian–Triassic facies zones in terrane reconstructions in the Alpine-North Pannonian Domain. Tectonophysics 242, 19–40.

Hartmann, J., Moosdorf, N., 2012. The new global lithological map database GLiM: a representation of rock properties at the Earth surface. Geochem. Geophys. Geosyst. 13, Q12004. http://dx.doi.org/10.1029/2012GC004370.

Holland, H.D., 1978. The Chemistry of the Atmosphere and Oceans. Wiley Interscience, New York.

Hren, M.T., Hilley, G.E., Page Chamberlain, C., 2007. The relationship between tectonic uplift and chemical weathering rates in the Washington cascades: field measurements

and model predictions. Am. J. Sci. 307, 1041–1063. http://dx.doi.org/10.2475/09.2007.01.
Huh, Y., 2010. Estimation of atmospheric CO_2 uptake by silicate weathering in the Himalayas and the Tibetan Plateau: a review of existing fluvial geochemical data. Monsoon evolution and tectonics-climate linkage in Asia. Geol. Soc. Lond. Spec. Publ. 342, 129–151.
IAEA, 1981. Stable isotope hydrology. Deuterium and oxygen-18 in water cycle. In: Gat, J.R., Gonfiantini, R. (Eds.), Technical Report. International Atomic Energy Agency, Wien.
IUGS Subcommission on the systematics of the Igneous Rocks, 1973. Classification and nomenclature of the plutonic rocks. Neues Jahrb. Mineral. Monatshefte 149–164.
Le Bas, M.J., Le Maitre, R.W., Streckeisen, A., Zanettin, R., 1986. A chemical classification of volcanic rocks based on the total alkali–silica diagram. J. Petrol. 27 (3), 745–750.
Li, G., Elderfield, H., 2013. Evolution of carbon cycle over the past 100 million years. Geochim. Cosmochim. Acta 103, 11–25. http://dx.doi.org/10.1016/j.gca.2012.10.014.
Li, G., Ji, J., Chen, J., Kemp, D.B., 2009. Evolution of the Cenozoic carbon cycle: the roles of tectonics and CO_2 fertilization. Glob. Biogeochem. Cycles 23, GB1009. http://dx.doi.org/10.1029/2008GB003220.
Longinelli, A., Selmo, E., 2003. Isotopic composition of precipitation in Italy: a first overall map. J. Hydrol. 270, 75–88.
Louvat, P., Allègre, C.J., 1997. Present denudation rates at Réunion Island determined by river geochemistry: basalt weathering and mass budget between chemical and mechanical erosions. Geochim. Cosmochim. Acta 61, 3645–3669.
Knoll, M.A., James, W.C., 1987. Effect of the advent and diversification of vascular land plants on mineral weathering through geologic time. Geology 15, 1099–1102.
Kump, L.R., Brantley, S.L., Knoll, M.A., 2000. Chemical weathering, atmospheric CO_2, and climate. Annu. Rev. Earth Planet. Sci. 28, 611–667. http://dx.doi.org/10.1146/annurev.earth.28.1.611.
Kump, L.R., Kasting, J.F., Crane, R.G., 2009. The Earth System. 3rd edition. Prentice Hall (432 pp.).
Mackenzie, F.T., Garrels, R.M., 1966. Chemical mass balance between rivers and oceans. Am. J. Sci. 264, 507–525. http://dx.doi.org/10.2475/ajs.264.7.507.
Mackenzie, F.T., Kump, L.R., 1995. Reverse weathering, clay mineral formation, and oceanic element cycles. Science 270, 586–587. http://dx.doi.org/10.1126/science.270.5236.586.
Marchina, C., Bianchini, G., Natali, C., Pennisi, M., Colombani, N., Tassinari, R., Knoeller, K., 2014. The Po river water from the Alps to the Adriatic Sea (Italy): new insights from geochemical and isotopic ($\delta^{18}O$-δD) data. Environ. Sci. Pollut. Res. 22 (7), 5184–5203. http://dx.doi.org/10.1007/s11356-014-3750-6.
Meybeck, M., 1986. Composition chimique naturelle des ruisseaux non pollués en France. Sci. Géol. Bull. 39, 3–77.
Meybeck, M., 1987. Global chemical weathering of surficial rocks estimated from river dissolved load. Am. J. Sci. 287, 401–428.
Meybeck, M., 2003. Global occurrence of major elements in rivers. Surface and Ground Water, Weathering, and Soils. Treatise on Geochemistry, Volume 5. Editor: J.I. Drever. Executive Editors: H.D. Holland and K.K. Turekian. Elsevier, 207–224 p.
Michalopoulos, P., Aller, R.C., 1995. Rapid clay mineral formation in amazon delta sediments: reverse weathering and oceanic elemental cycles. Science 270, 614–617.
Michalopoulos, P., Aller, R.C., 2004. Early diagenesis of biogenic silica in the amazon delta: alteration, authigenic clay formation, and storage. Geochim. Cosmochim. Acta 68, 1061–1085. http://dx.doi.org/10.1016/j.gca.2003.07.018.
Millot, R., Gaillardet, J., Dupré, B., Allègre, C.J., 2002. The global control of silicate weathering rates and the coupling with physical erosion: new insights from rivers of the Canadian Shield. Earth Planet. Sci. Lett. 196, 83–98.
Misra, S., Froelich, P.N., 2012. Lithium isotope history of cenozoic seawater: changes in silicate weathering and reverse weathering. Science 335, 818–823. http://dx.doi.org/10.1126/science.1214697.
Mitchell, T., Jones, P.D., 2005. An improved method of constructing a database of monthly climate observations and associated high-resolution grids. Int. J. Climatol. 25, 693–712.
Mortatti, J., Probst, J.L., 2003. Silicate rock weathering and atmospheric/soil CO_2 uptake in the Amazon Basin estimated from river water geochemistry: seasonal and spatial variations. Chem. Geol. 197, 177–196.
Mosello, R., Barbieri, A., Brizzio, M.C., Calderoni, A., Marchetto, A., Passera, S., Rogora, M., Tartari, G., 2001. Nitrogen budget of Lago Maggiore: the relative importance of atmospheric deposition and catchment sources. J. Limnol. 60 (1), 27–40.
Neteler, M., Mitasova, H., 2008. Open source GIS: a GRASS GIS approach. Third edition The International Series in Engineering and Computer Science vol. 773. Springer, New York (406 pp.).
Nisi, B., Vaselli, O., Buccianti, A., Minissale, A., Delgado Huertas, A., Tassi, F., Montegrossi, G., 2008. Geochemical and isotopic investigation of the dissolved load in the running waters from the Arno Valley: evaluation of the natural and anthropogenic input. Mem. Descrittive Carta Geol. Ital. LXXIX, 1–91.
Noh, H., Huh, Y., Qin, J., Ellis, A., 2009. Chemical weathering in the Three Rivers Region of eastern Tibet. Geochim. Cosmochim. Acta 73, 1857–1877.
Olivier, J.-M., Carrel, G., Lamouroux, N., Dole-Olivier, M.-J., Mallard, F., Bravard, J.-P., Amoros, C., 2009. The Rhône River Basin. In: Tockner, K., Robinson, C., Uehlinger, U. (Eds.), Rivers of Europe. Academic Press, pp. 247–295.
Pearson, K., 1895. Notes on regression and inheritancein the case of two parents. Proc. R. Soc. Lond. 58, 240–242.
Peripoli, G., 2008. Chemical characterization of Adige River along longitudinal gradients. Tesi di laurea. Università di Padova.
Pinet, P., Souriau, M., 1988. Continental erosion and large-scale relief. Tectonics 7, 563–582.
Probst, J.L., 1992. Géochimie de l'érosion continentale: mécanismes, bilance global actuel et fluctuations au cors des 500 dernier millions d'années. Sci. Géol. Mém. Strasbourg 94, 161.
Probst, J.L., Mortatti, J., Tardy, Y., 1994. Carbon river fluxes and global weathering CO_2 consumption in the Congo and Amazon River Basins. Appl. Geochem. 9, 1–13.
Quantum GIS Development Team, 2012. Quantum GIS geographic information system. Open source geospatial foundation project. http://qgis.osgeo.org.
R Core Team, 2015. R: a language and environment for statistical computing. R Foundation for Statistical Computing, Vienna, Austria (URL http://www.R-project.org/).
Rogora, M., Mosello, R., Arisci, S., Brizzio, M., Barbieri, A., Balestrini, R., Waldner, P., Schmitt, M., Stähli, M., Thimonier, A., Kalina, M., Puxbaum, H., Nickus, U., Ulrich, E., Probst, A., 2006. Atmospheric deposition on the Alps: effects on the functioning of the alpine and subalpine ecosystems. Hydrobiologia 562, 17–40.
Roy, S., Gaillardet, J., Allègre, C.J., 1999. Geochemistry of dissolved and suspended loads of the Seine river, France: anthropogenic impact, carbonate and silicate weathering. Geochim. Cosmochim. Acta 63, 1277–1292.
Schmid, S.M., Fügenschuh, B., Kissling, E., Schuster, R., 2004. Tectonic map and overall architecture of the Alline orogen. Eclogae Geol. Helv. 97, 93–117.
Schwartzman, D.W., Volk, T., 1989. Biotic enhanchement of weathering and habitability of earth. Nature 340, 457–460.
Semhi, K., Probst, J.L., Etcheber, H., Bazerbachi, A., 1993. Dissolved river transport in the Garonne Basin, seasonal and interannual variations. EUG VII, Strasbourg, Abstract supplement n.1 to Terra Nova 5, p. 633.
Sillen, L.G., 1967. The ocean as a chemical system. Science 156, 1189–1197.
Spearman, C., 1904. The proof and measurement of association between two things. Am. J. Psychol. 15, 72–101.
Stampfly, G., Mosar, J., Favre, P., Pillevuit, A., Vannay, J.C., 2001. Permo-Mesozoic Evolution of the Western Tethys Realm: the Neo-Tethys East Mediterranean Basin Connection. Peri-Tethys Memoir 6: Peri-Tethyan Rift/Wrench Basins and Passive Margins. Mém. Mus. Natn. Hist. Nat. Paris 51, pp. 108–186.
Stefanini, S., 1976. Composizione delle acque fluviali del Friuli-Venezia Giulia durante la fase di magra e di piena dei corsi d'acqua. Quad. Ist. Ric. Sulle Acque 28, 386–450.
Tachikawa, T., Kaku, M., Iwasaki, A., 2011. ASTER GDEM Version 2 Validation Report. Report to the ASTER GDEM Version 2 Validation Team.
Tardy, Y., 1986. Le cycle de l'eau. Climats, Paléoclimates et Géochimie Globale. Masson, Paris.
Tipper, E.T., Bickle, M.J., Galy, A., West, A.J., Pomiés, C., Chapman, H.J., 2006. The short-term climatic sensitivity of carbonate and silicate weathering fluxes: insight from seasonal variations in river chemistry. Geochim. Cosmochim. Acta 70, 2737–2754. http://dx.doi.org/10.1016/j.gca.2006.03.005.
Torres, M.A., West, A.J., Li, G., 2014. Sulphide oxidation and carbonate dissolution as a source of CO_2 over geological timescales. Nature 507, 346–349.
Tricart, P., 1984. From passive margin to continental collision: a tectonic scenario for the Western Alps. Am. J. Sci. 284, 97–120.
Trümphy, R., 1960. Paleotectonic evolution of the Central and Western Alps. Bull. Geol. Soc. Am. 71, 843–908.
Uehlinger, U., Wantzen, K.M., Leuven, R.S.E.W., Arndt, H., 2009. The Rhine River Basin. In: Tockner, K., Robinson, C., Uehlinger, U. (Eds.), Rivers of Europe. Academic Press, pp. 199–245.
Velbel, M.A., 1993. Temperature dependence of silicate weathering in nature: how strong of a negative feed Back on long-term accumulation of atmospheric CO_2 and global greenhouse warning? Geology 21, 1059–1062.
Verbunt, M., Gurtz, J., Kasper, K., Lang, H., Warmerdam, P., Zappa, M., 2003. The hydrological role of snow and glaciers in alpine river basins and their distributed modeling. J. Hydrol. 282, 36–55.
Viers, J., Oliva, P., Dandurand, J.L., Dupré, B., Gaillardet, J., 2007. Chemical weathering rates, CO_2 consumption, and control parameters deduced from the chemical composition of rivers. In: Surface and Ground Water, Weathering, and Soils. Treatise on Geochemistry, Volume 5. Editor: J.I. Drever. Executive Editors: H.D. Holland and K.K. Turekian. Elsevier, p. 1–25.
Viviroli, D., Weingartner, R., 2004. The hydrological significance of mountains: from regional to global scale. Hydrol. Earth Syst. Sci. 8, 1016–1029.
Walker, J.C.G., Hayes, P.B., Kasting, J.F., 1981. A negative feedback mechanism for the long-term stabilization of the earth's surface temperature. J. Geophys. Res. 86, 9776–9782.
Weingartner, R., Viviroli, D., Schädler, B., 2007. Water resources in mountain regions: a methodological approach to assess the water balance in a highland–lowland system. Hydrol. Process. 21, 578–585.
White, A.F., 2003. Natural weathering rates of silicate minerals. Surface and Ground Water, Weathering, and Soils. Treatise on Geochemistry, Volume 5. Editor: J.I. Drever. Executive Editors: H.D. Holland and K.K. Turekian. Elsevier, p. 133–168.
White, A.F., Blum, A.E., 1995. Effects of climate on chemical weathering in watersheds. Geochim. Cosmochim. Acta 59, 1729–1747.
Yang, C.K., Telmer, K., Veizer, J., 1996. Chemical dynamics of the 'St. Lawrence' riverine system; δD_{H2O}, $\delta^{18}O$, δC_{dic}, $\delta^{34}S_{sulfate}$ and dissolved $^{87}Sr/^{86}Sr$. Geochim. Cosmochim. Acta 60, 851–866.

Web references

http://www.swisstopo.admin.ch - 18.03.2105
http://one.geology.cz/ - 18.03.2105
http://www.isprambiente.gov.it - 18.03.2105